

RESEARCH

Open Access



Fecal microbiota transplantation attenuates Alzheimer's disease symptoms in APP/PS1 transgenic mice via inhibition of the TLR4-MyD88-NF- κ B signaling pathway-mediated inflammation

Xiang Li^{1,2,3,5*}, Qingyong Ding^{1,2,3,4†}, Xinxin Wan^{1,2,3,5}, Qilong Wu^{1,2,3,5}, Shiqing Ye^{1,2,3,5} and Yongliang Lou^{1,2,3,5*}

Abstract

Alzheimer's disease (AD) is a prevalent and progressive neurodegenerative disorder that is the leading cause of dementia. The underlying mechanisms of AD have not yet been completely explored. Neuroinflammation, an inflammatory response mediated by certain mediators, has been exhibited to play a crucial role in the pathogenesis of AD. Additionally, disruption of the gut microbiota has been found to be associated with AD, and fecal microbiota transplantation (FMT) has emerged as a potential therapeutic approach. However, the precise mechanism of FMT in the treatment of AD remains elusive. In this study, FMT was performed by transplanting fecal microbiota from healthy wild-type mice into APP/PS1 mice (APP^{swe}, PSEN1^{dE9}) to assess the effectiveness of FMT in mitigating AD-associated inflammation and to reveal its precise mechanism of action. The results demonstrated that FMT treatment improved cognitive function and reduced the expression levels of inflammatory factors by regulating the TLR4/MyD88/NF- κ B signaling pathway in mice, which was accompanied by the restoration of gut microbial dysbiosis. These findings suggest that FMT has the potential to ameliorate AD symptoms and delay the disease progression in APP/PS1 mice.

Keywords Alzheimer's disease, Inflammation, Fecal microbiota transplantation, Intestinal microbiota, Short-chain fatty acids, Microbiota-gut-brain axis

[†]Xiang Li and Qingyong Ding contributed equally to this study.

*Correspondence:

Xiang Li

yhx2008@163.com

Yongliang Lou

louyongliang2013@163.com

¹Wenzhou Key Laboratory of Sanitary Microbiology; School of Laboratory Medicine and Life Sciences; Key Laboratory of Laboratory Medicine, Ministry of Education, Wenzhou Medical University, Wenzhou, Zhejiang Province, China

²Colorectal Cancer Research Center, Wenzhou Medical University, Wenzhou, Zhejiang Province, China

³One Health Research Institute, Wenzhou Medical University, Wenzhou, Zhejiang Province, China

⁴Testing Center of the First Affiliated Hospital of Anhui University of Chinese Medicine, Hefei, Anhui Province, China

⁵Zhejiang Provincial Key Laboratory of Medical Genetics, School of Laboratory Medicine and Life Sciences, Wenzhou Medical University, Wenzhou, Zhejiang Province, China



Introduction

Alzheimer's disease (AD), a progressive neurodegenerative disease, is characterized by the presence of β -amyloid ($A\beta$) plaques and neurogenic fibrillary tangles formed by hyperphosphorylated Tau proteins in cortical and hippocampal regions of the brain [1]. Its primary clinical manifestations involve diminished cognitive function, memory loss, and executive dysfunction [2]. The etiology of AD is complex, and its pathogenesis remains the subject of ongoing investigation, with multiple hypotheses being postulated. These include the $A\beta$ plaque and Tau protein hypothesis [3], the cholinergic hypothesis [4], neuroinflammation [5], oxidative stress [6], and mitochondrial autophagy [7]. Among them, microglial activation and neuroinflammation emerge as pivotal factors in the pathogenesis of AD [8, 9]. A growing body of evidence demonstrated that the gut microbiota regulates brain function, and the microbiota-gut-brain axis (MGBA) underscores its function as a bidirectional communication system that facilitates the interaction between the gut and the brain [10]. The MGBA encompasses multiple communication pathways, involving the immune system, the vagus nerve, the enteric nervous system, and fluctuations in microbial metabolites, notably short-chain fatty acids (SCFAs) [11]. SCFAs and other metabolites produced by intestinal flora may directly or indirectly impact brain function [12]. Neuroinflammation and changes in blood-brain-barrier (BBB) permeability may result in deregulation of these pathways [13]. APP/PS1 mice carry two transgenes associated with Alzheimer's Disease (AD)-associated mutations: chimeric mice/human APP with Swedish mutations and human PSEN1 with missing exon 9 (dE9), both of which are controlled by the mouse prion protein (*Prnp*) gene promoter. In addition, amyloid plaques in the cerebral cortex of this model mouse began to appear at about 4 months of age and in the hippocampus at about 6 months of age [14]. Besides, as mice grow older, their memory and cognitive deficits can be detected by the Morris Water Maze experiment (MWM) [14].

Patients with AD frequently exhibit diminished microbial diversity and a modified composition of the gut microbiota. This includes an elevation in the abundance of Bacteroidetes and a reduction in the levels of Firmicutes [15]. In patients with cognitive dysfunction, an increased ratio of pro-inflammatory bacteria, including *Shigella/Escherichia* ratio, was found, along with a decreased presence of anti-inflammatory gut microbiota, specifically *Escherichia coli* [16]. Dysregulated intestinal microecology triggers chronic inflammation in the gut [17]. This intestinal inflammation can lead to compromised integrity and permeability of the intestinal barrier [18], enabling pro-inflammatory factors to translocate across the intestinal barrier into the systemic circulation

and subsequently enter the brain via the MGBA, leading to neuroinflammation [19]. The levels of inflammatory factors, such as interleukin-1 (IL-1), interleukin-6 (IL-6), and tumor necrosis factor- α (TNF- α) were significantly higher in AD patients, highlighting their crucial role in neuroinflammation [20, 21]. Another study found that levels of bacterial lipopolysaccharides were noticeably higher in the brains of AD patients [22]. However, the elevation of pro-inflammatory factors in the brains of APP/PS1 mice carrying Toll-like receptor 4 (TLR4) mutations was mitigated, suggesting that TLR4 plays a regulatory role in the expression levels of pro-inflammatory cytokines in APP/PS1 mice [23]. As a result, the specific roles of TLR4-related signaling pathways and gut microbiota in the pathogenesis of AD should be further explored to provide novel therapeutic techniques for AD.

In recent years, fecal microbiota transplantation (FMT) has exhibited to play a pivotal role in numerous diseases, such as *Clostridium difficile* infection, irritable bowel disease, irritable bowel syndrome, etc [24]. The existing research has concentrated on investigating the impact of these changes on neurological diseases [25]. The precise mechanism of FMT treatment for most diseases remains elusive, however, it may be related to the increased microbial abundance and diversity, a higher number of beneficial bacteria, and the enhanced immunological function of the body [26]. Memory deficits and higher levels of pro-inflammatory cytokines were found in normal C57BL/6 mice that received fecal transplants from 5xFAD mice [27]. Furthermore, FMT therapy alleviated cognitive deficits in APP/PS1 mice, reduced $A\beta$ deposition, and reversed microbiota and SCFA changes [28]. However, further research is required to investigate the specific mechanisms and therapeutic effects of FMT on the treatment of AD.

To investigate the potential therapeutic effects of FMT on AD, FMT was performed by transferring fecal microbiota from healthy wild-type mice to APP/PS1 mice. This study aimed to evaluate the protective impact of FMT against AD and elucidate the associated mechanisms. Different metabolites were utilized to treat lipopolysaccharide (LPS)-induced Fetal Human Colon (FHC) cells and Mouse microglia (BV-2), in order to detect changes in the expression levels of inflammation-related proteins. It was hypothesized that in APP/PS1 mice, an imbalance of the gut microbiota could cause excessive production of pro-inflammatory cytokines, which, in combination with disruption of the intestinal barrier, could ultimately exacerbate the progression of AD via the MGBA.

Materials and methods

Animals

In this study, 3-month-old adult male APP/PS1 (APP^{swe}, PSEN1^{dE9}) double transgenic mice and age-matched

wild-type mice were utilized and purchased from Hangzhou Ziyuan Laboratory Animal Technology Co., Ltd. (Hangzhou, China). Mice were housed in a specific pathogen-free environment (22 ± 3 °C; humidity, $55 \pm 5\%$) under a light/dark cycle of 12:12. Food and water were available ad libitum. All animal protocols were approved

by the Experimental Animal Ethics Committee of Wenzhou Medical University (Approval No. wydy2022-0375).

Experimental design

The experimental design of the study is presented in Fig. 1A. After one month of standard housing conditions, experimental mice were randomly divided into 3 groups

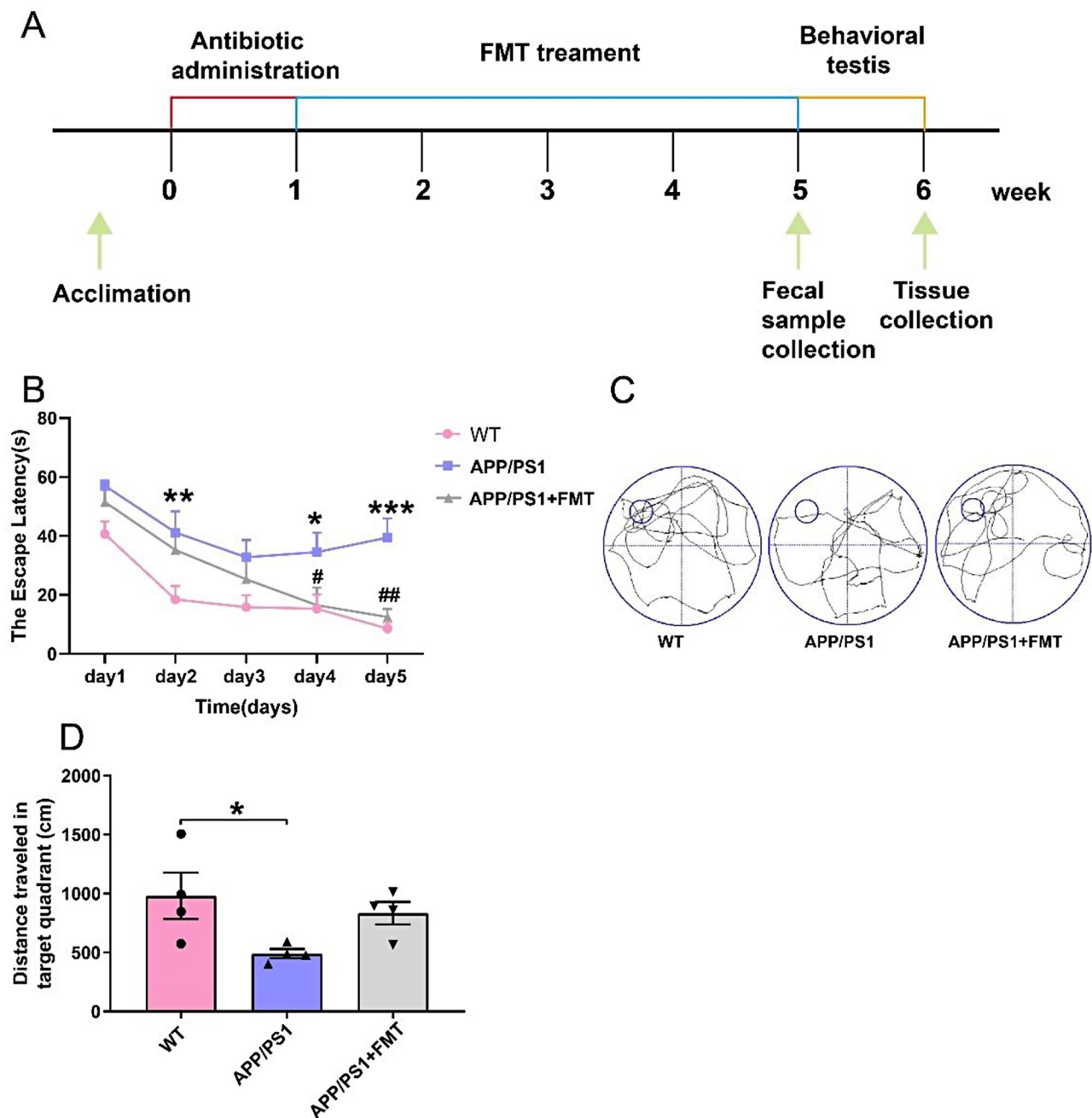


Fig. 1 Cognitive and behavioral changes in APP/PS1 mice treated with FMT. **(A)** Experimental protocol for FMT treatment. **(B)** Escape latency of mice during the training period of the MWM test ($n=6$ for each group). **(C)** Representative swimming routes in the platform-free exploration period of the MWM test. **(D)** Distance traveled through the target quadrant in the MWM test ($F=3.893$; $P=0.0605$; $df=11$) ($n=4$ for each group). Data were analyzed using one-way ANOVA, followed by Dunnett's multiple comparisons test **(D)** and repeated measures ANOVA, followed by Tukey's multiple comparisons test **(B)**. Data were expressed as mean \pm SEM. * $P < 0.05$, ** $P < 0.01$, *** $P < 0.001$ vs. WT group; # $P < 0.05$, ## $P < 0.01$ vs. APP/PS1 group

($n=8$ mice for each group): WT group, APP/PS1 group, and APP/PS1+FMT group. All experimental mice were given 200 μ l of the four antibiotics (200 mg/L neomycin, 200 mg/L ampicillin, 200 mg/L metronidazole, and 100 mg/L vancomycin) [29] daily for one week to eliminate the initial intestinal microorganisms. After one week of antibiotic treatment, mice in the APP/PS1+FMT group received a daily oral gavage of 200 μ l of freshly prepared fecal resuspension from WT mice for 4 weeks. Mice in the WT and APP/PS1 groups received an equivalent volume of saline. After 4 weeks, fresh fecal samples from all mice were collected and stored at -80°C . Mice were sacrificed at the end of the behavioral experiments and tissues were collected.

FMT procedure

Fresh fecal samples from wild-type mice were collected daily and dissolved in sterile saline at a 1:5 (W/V) ratio. The mixture was then filtered sequentially through a series of filters with pore sizes of 1.0, 0.5, and 0.25 mm. After filtration, the collected liquid was centrifuged at $4000 \times g$ for 5 min. The supernatant was collected as gavage fluid.

Morris water maze (MWM) test

The MWM test was conducted to evaluate the spatial learning ability and memory capacity of mice. The experimental setup included a circular water tank (100 cm in diameter, 50 cm in height, and 30 cm deep) and a removable platform that was hidden 1 cm underwater. The water temperature was maintained at $18\text{--}22^{\circ}\text{C}$. Each day, mice were introduced into the pool from various starting positions within the four quadrants. Training sessions were carried out four times daily over a span of five days, and each session was performed at 30-min interval. The objective of the training was to locate the submerged platform. The instrument automatically calculated the time taken to reach the platform for the first time within 1 min. If mice did not reach the platform in the allocated time, they were directed to the submerged platform and forced to stand there for 10 s. The invisible platform was removed on the last day. Mice were positioned farthest away from the target platform and allowed to swim freely in the tank for 60 s. The number of platform crossings and the path length were recorded using computer video analysis software (Shanghai Jiliang Software Science & Technology Co., Ltd., Shanghai, China).

Congo red staining and nissl staining

Adult mice were anesthetized after the behavioral experiment, and they promptly received phosphate-buffered saline (PBS, pH 7.4), followed by 4% paraformaldehyde for cardiac perfusion. Tissue samples fixed with 4% paraformaldehyde were sequentially immersed in ethanol

with varying concentrations: 70% for 12 h, 80% for 1 h, 90% for 1 h, 95%(I)for 1 h, 95%(II)for 1 h, 100%(I)for 1 h, and 100%(II) for 1 h. Subsequently, they were subjected to two cycles of 100% xylene, each lasting for 15 min, followed by incubation in soft wax I and soft wax II, each for 1 h, and finally embedded into hard wax. Tissues were paraffin-embedded and cut into 5- μ m sections for further staining experiments. Slides were dewaxed at 65°C for 2 h, and treated with xylene I for 5 min, xylene II for 5 min, ethanol (100%) for 2 min twice, ethanol (100%) for 2 min, ethanol (95%) for 2 min, ethanol (80%) for 2 min, ethanol (70%) for 2 min, ethanol (50%) for 2 min, and distilled water for 2 min.

Congo red staining: Highman Congo red staining solution (G1535, Solarbio, Beijing, China) was applied to brain tissue slices for 10 min, followed by utilization of alkaline differentiation solution for 10 s. The differentiation was terminated by placing the sections in water, followed by rinsing them with running water. Subsequently, the sections were immersed in Lillie-Mayer hematoxylin staining solution for 2 min, rinsed slightly with running water, and washed with distilled water to achieve a blue differentiation. The sections were then dehydrated through an ethanol gradient, made transparent with xylene, and finally sealed with resin. The quantification of amyloid plaques was conducted under a microscope.

Nissl staining: The 5 μ m-thick brain tissue sections were initially deparaffinized following the previously outlined protocol. Subsequently, they were stained for 1 h at 56°C using a cresyl violet staining solution (G1430, Solarbio). The stained sections were then washed with deionized water, subjected to differentiation for approximately 2 min using differentiation solution, rapidly dehydrated with absolute ethanol, cleared in xylene, and finally sealed with resin. Microscopy was used to count the number of amyloid plaques and Nissl bodies.

Hematoxylin-eosin (HE) staining and alcian blue-nuclear-fast red staining

HE staining

The paraffin-embedded colon tissue was sectioned into 5 μ m-thick slices, which were then subjected to the following steps: dewaxed at 65°C for 2 h, treated with xylene I for 5 min, followed by xylene II for further 5 min. The sections were subsequently immersed in ethanol (100%) for 2 min (repeated twice), ethanol (95%) for 2 min, ethanol (80%) for 2 min, ethanol (70%) for 2 min, 50% ethanol for 2 min, and finally distilled water for 2 min. They were then stained with hematoxylin (C0105S-2; Beyotime, Shanghai, China) for 10 min, rinsed with tap water for 10 min, distilled water for 30 s, and fractionated in a hydrochloric acid ethanol fractionation solution for 30 s. After rinsing with running water for 10 min and distilled water for 30 s, the sections were

sequentially immersed in ethanol (50%) for 2 min, ethanol (70%) for 2 min, ethanol (80%) for 2 min, and ethanol (95%) for 2 min. Following this, they were stained with eosin (C0105S-1; Beyotime) for 10 s and subsequently treated with ethanol (95%) for 2 min (repeated twice), and ethanol (100%) for 2 min (also repeated twice). The sections were then cleared using xylene and finally sealed with resin. Under the microscope, histomorphological changes were observed and the tissues were evaluated according to the criteria [30].

Alcian blue-nuclear-fast red staining: The 5 μ m-thick sections were subjected to the dewaxing process as previously described, followed by immersion in ethanol (100%) for 5 min, ethanol (90%) for 2 min, ethanol (80%) for 2 min, and ethanol (70%) for an additional 2 min. The rehydrated slides were placed in a wet box, stained for 1 h with 100 μ L Alcian blue staining solution (C0155S, Beyotime), thrice rinsed with distilled water, and subsequently stained with 100 μ L nuclear solid red staining solution for 10 min. The staining solution was carefully removed, and the sections were subsequently rinsed with tap water for 5 min. They were sequentially immersed in ethanol (70%) for 10 s, ethanol (80%) for 10 s, ethanol (90%) for 10 s, and finally ethanol (100%) for 10 s. Following this, the sections were made transparent by submersion in xylene for 1 min before being sealed with resin. Densitometric analysis of the Alcian blue-positive area in the colon was carried out under a microscope.

Quantitative reverse transcription polymerase chain reaction (RT-qPCR)

RNA was extracted from hippocampal and colonic tissues of mice using the RNAiso Plus reagent (9109; TaKaRa, Beijing, China). For reverse transcription, the PrimeScript™ RT kit with gDNA Eraser (RR047A, TaKaRa) was utilized, and TB Green® Premix Ex Taq™ II (RR820A, TaKaRa) was used to detect inflammatory genes. The specific paired primers synthesized by Beijing Qingke Biotechnology Co., Ltd. (Beijing, China) were summarized as follows: tumor necrosis factor- α (TNF- α):5'-TGAGATCCATGCCGTTGGC-3' (antisense),5'-CACGTCGTAGCAAACCACC-3'(sense); interleukin-6(IL-6):5'-AAGTGCATCATCGTTCATAC A-3' (antisense),5'-AGGATACCACTCCCAACAGAC C-3' (sense); interleukin-1 β (IL-1 β): 5'-TGCTGCGGGAT TTGAAGCTG-3' (antisense),5'-AATGCCACCTTTTG ACAGTGAT-3' (sense); β -actin: 5'-CGCTCGTTGCCA ATAGTG-3'(antisense),5'-GCTGTGCTATGTTGCTCT AG-3' (sense). The CFX96™Real-Time system (Bio-Rad Laboratories Inc., Hercules, CA, USA) was used to detect the expression levels of inflammatory genes in colonic and hippocampal tissues. The RT-qPCR was conducted under the following conditions: pre-denaturation at 95 °C for 30 s, followed by 40 cycles of denaturation at 95 °C for

5 s, and annealing/extension at 60 °C for 30 s. The relative mRNA expression of inflammatory factors was calculated by the $2^{-\Delta\Delta C_t}$ method.

Enzyme-linked immunosorbent assay (ELISA) for cytokine detection

Eyeballs were removed from mice to collect blood, and the separated plasma was stored at -80 °C for later use. ELISA kits (Dakewe Biotech Co., Ltd., Shanghai, China) were utilized for testing inflammatory factors, such as IL-6 (Cat#:1210602), IL-1 β (Cat#:1210122), and TNF- α (Cat#:1217202). Experiments were performed according to the manufacturer's instructions. Readings were taken with a multifunctional enzyme marker (SpectraMax M5; Molecular Devices Shanghai Co., Ltd., Shanghai, China) at the wavelength of 450 nm.

Western blotting

Hippocampal and colonic tissues were lysed for 10 min in lysis buffer (Beyotime), and the recovered protein supernatant was centrifuged at 12,000 g for 20 min. The BCA Protein Concentration Assay kit (P0010, Beyotime) was utilized to measure protein concentration in tissues. Protein samples were separated by well-prepared SDS-PAGE gel and electro-transferred at a low temperature to PVDF membranes (Merck Millipore Ltd., Darmstadt, Germany). Membranes were shaken for 2 h in 5% skim milk before being incubated overnight at 4 °C with the primary antibody. The membranes were subsequently incubated for 2 h with secondary antibodies (horseradish peroxidase-labeled goat anti-mouse IgG (H+L) (1:2500, A0216, Beyotime) and horseradish peroxidase-labeled goat anti-rabbit IgG (H+L) (1:2500, A0208, Beyotime). Proteins were detected using the Ultrasensitive ECL Chemiluminescence kit (P10100, New Cell & Molecular Biotech Co., Ltd., Beijing, China), and band densities were analyzed by a Chemiluminescent imaging system (Bio-Rad Laboratories Inc.).

The following primary antibodies were utilized: anti-ZO-1 (1:1000, AF5145, Affinity), anti-Occludin (1:1000, R1510-33, HUABIO), anti-Claudin 1 (1:1000, RT1141, HUABIO), anti-TLR4 (1:1000, A5258, ABclonal), anti-MyD88 (1:1000, AF7524, Beyotime), anti-NF- κ B p65 (1:5000, CY5034, Abways), anti-COX-2 (1:1000, db8534, Diagbio), anti-IL-6 (1:1000, db7166, Diagbio), anti-IL-1 β (1:1000, AF5103, Affinity), anti-TNF- α (1:1000, AF7014, Affinity), anti-APP (1:1000, AF6219, Beyotime), anti-p-Tau (1:1000, ET1611-68, HUABIO), β -Actin (1:3000, AB0035, Abways), and GAPDH (1:2000, db106, Diagbio).

Microbial community diversity sequencing

Fresh mouse fecal samples were aseptically collected in sterile EP tubes, and DNA was extracted using the OMEGA Soil DNA kit (M5636-02) from Omega Bio-Tek

(Norcross, GA, USA). Subsequently, the V3-V4 regions of fecal microbial genes were amplified with primers (Forward: ACTCCTACGGGAGGCAGCA, Reverse: GGACTACHVGGGTWTCTAAT). Paired-end sequencing of community DNA fragments was conducted on the Illumina NovaSeq platform, which was provided by Shanghai Personalbio Technology Co., Ltd. (Shanghai, China). Data preprocessing, including de-priming, quality filtering, denoising, sequence splicing, and chimera removal, was executed using the DADA2 method [31]. Each sequence obtained after de-duplication and quality control with DADA2 was defined as a signature sequence, representing the OTU sequence. Bacterial gene annotation and subsequent taxonomic analysis were carried out by Shanghai Personalbio Technology Co., Ltd. The database is gg_13. The data standardization method used in heat map drawing: the samples have been clustered using the UPGMA method (default clustering algorithm) based on the Euclidean distance of their species composition data, and are arranged according to the clustering results by default; otherwise, they are arranged in the default order of samples/groups. By default, the species are also clustered using the UPGMA method (default clustering algorithm) based on their Pearson correlation coefficient matrix derived from the composition data, and are arranged according to the clustering results; otherwise, they are sorted based on their average abundance across the samples/groups.

Gas chromatography-mass spectrometry (GC-MS) analysis of metabolites

The sample was placed in a 1.5 mL centrifuge tube containing 500 μ L of water and 100 mg of glass beads. It was agitated for 1 min and subsequently centrifuged for 10 min at 12,000 rpm. The resulting supernatant was thoroughly mixed with a solution consisting of 15% phosphoric acid (100 μ L), an internal standard (4-methylvaleric acid) solution at a concentration of 375 μ g/mL (20 μ L), and ether (280 μ L). After another 10-min of centrifugation at 12,000 rpm (at 4 °C) [32], the supernatant was prepared for machine analysis. The Trace 1300 gas chromatograph (Thermo Fisher Scientific, Waltham, MA, USA) was employed for the analysis. An Agilent HP-INNOWAX capillary column (30 m \times 0.25 mm ID \times 0.25 μ m) was used. The sample was injected with a split flow of 1 μ L and a split ratio of 10:1.

The instrument was programmed to begin at 90 °C, increase to 120 °C at a rate of 10 °C/min, then to 150 °C at a rate of 5 °C/min, and finally to 250 °C at a rate of 25 °C/min, where it was maintained for 2 min. Helium was utilized as the carrier gas with a flow rate of 1.0 mL/min. Metabolite analysis was carried out using a Thermo ISQ 7000 mass spectrometer (Thermo Fisher Scientific) operating in the electron impact ionization mode with

an electron energy of 70 eV [33, 34]. Calibration curves were created by plotting the concentrations of the standards along the X-axis and representing the ratio of the peak areas of the standards to the internal standards along the Y-axis. These calibration curves were used to quantitatively determine metabolite concentrations of all samples.

Cell culture

FHC cells and BV2 microglia were cultured in a CO₂ incubator at 37 °C in a Dulbecco's modified Eagle's medium supplemented with 10% fetal bovine serum (FBS) and a 1% penicillin-streptomycin solution (100 \times). Various concentrations of sodium propionate (SP) were applied to the cells, and the final concentration was determined using the cell counting kit-8 (CCK-8) assay. Subsequently, SP doses were administered to cells induced by LPS, and the levels of proteins related to the NF- κ B inflammatory signaling pathway and inflammatory factors were determined through Western blot analysis.

Statistical analysis

GraphPad Prism 8.0 software (GraphPad Software, Inc., San Diego, CA, USA) was used to perform the statistical analysis, and data were expressed as the mean \pm standard deviation (SD) of the mean of at least three independent experiments. All datasets were tested for normal distribution by the Shapiro-Wilk test. For normally distributed data, one-way analysis of variance (ANOVA) was used to determine significant differences among the three groups, followed by Tukey's multiple comparisons test. If one or more groups in the one-way ANOVA dataset deviated from a normal distribution, Kruskal-Wallis test was conducted, followed by Dunn's multiple comparisons. In the analysis of variations in metabolites between groups, two-tailed unpaired t-test was applied when both datasets adhered to a Gaussian distribution. In addition, repeated measures ANOVA was performed on the escape latency data from the MWM test. *P*-value less than 0.05 was considered statistically significant. Microbiome bioinformatics was conducted using the QIIME2 2019.4 system [35] with slight modifications. The sequence data analysis was carried out by the QIIME2 and the R package (ver. 3.2.0).

Results

FMT treatment attenuates the impairment of cognitive and memory functions in AD mouse model

Cognitive impairment and short-term memory deficits are common symptoms of AD [36]. In the present study, the MWM test was employed to assess the impact of FMT on the learning and memory abilities of APP/PS1 mice, a common AD model. During the hidden platform phase, APP/PS1 mice exhibited significantly longer

escape latency compared to WT mice. In contrast, APP/PS1 mice treated with FMT (APP/PS1+FMT) showed escape latencies comparable to WT mice, indicating a notable improvement (Fig. 1B). Trajectory analysis during the exploratory phase revealed increased platform crossings in APP/PS1+FMT mice compared to APP/PS1 mice (Fig. 1C). Moreover, the distance traveled within the target quadrant was significantly shorter in APP/PS1 mice but restored in APP/PS1+FMT mice (Fig. 1D). These findings provide compelling evidence that FMT treatment could enhance spatial cognitive function and mitigate memory impairment in APP/PS1 mice.

FMT treatment restores dysregulated intestinal microbiota in APP/PS1 mice

The gut microbiota plays a crucial role in neurodegenerative diseases, such as AD [37]. Fecal samples from all groups of mice were subjected to 16 S rDNA sequencing to investigate whether FMT could induce alterations in the gut microbiota composition of APP/PS1 mice. The Chao1, Shannon, and Simpson indices were employed to characterize richness and diversity of species, in order to provide a more comprehensive assessment of the alpha-diversity of microbial communities. The analysis of alpha-diversity revealed no significant differences between the groups, as depicted in Fig. 2A. The β -diversity was calculated using the Bray-Curtis distance algorithm, and the results of the principal coordinates analysis (PCoA)

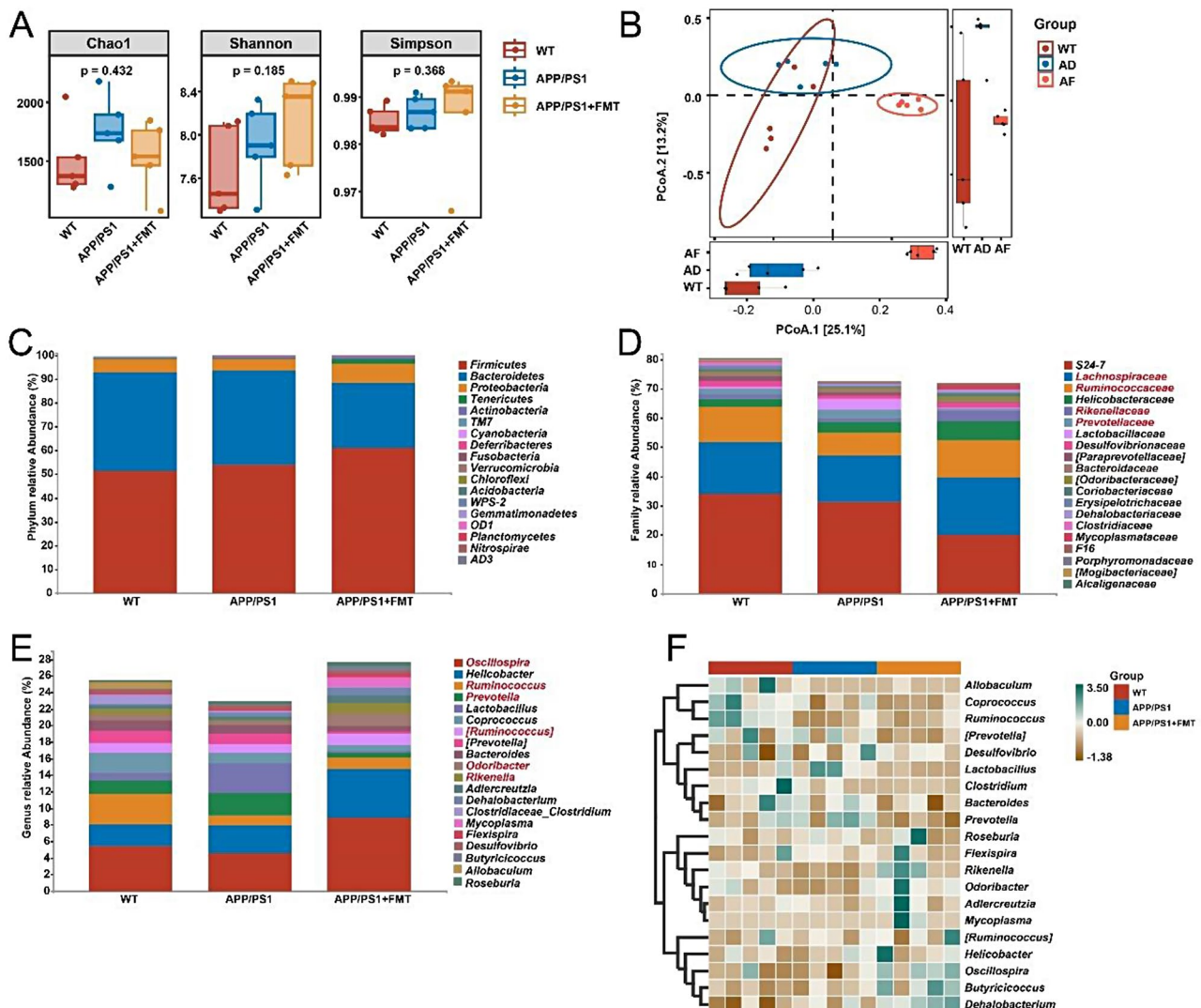


Fig. 2 Effects of FMT treatment on the dysregulation of intestinal microbiota in APP/PS1 mice. **(A)** Chao1 ($P=0.432$), Shannon ($P=0.185$) and Simpson ($P=0.368$) index analysis of alpha diversity of the gut microbiota ($n=5$ for each group). **(B)** PCoA distribution plot of the Bray-Curtis algorithm for beta diversity ($n=5$ for each group). **(C-E)** Relative abundance of intestinal flora at the phylum level, family level and genus level in different groups ($n=5$ for each group)(The parts marked in red are specifically mentioned). **(F)** Heat map of species composition at the genus level ($n=5$ for each group)

indicated distinct separations with varying distributions of gut microbiota among the groups (Fig. 2B). An investigation into the taxonomic composition of species was conducted to expand the exploration of the key bacteria contributing to the progression of AD. Major bacteria, such as Firmicutes, Bacteroidetes, Proteobacteria, Tenericutes, and Actinobacteria did not significantly differ at the phylum level (Fig. 2C). At the family level, APP/PS1 mice had lower abundances of Lachnospiraceae, Ruminococcaceae, and Rikenellaceae and a greater abundance of the proinflammatory bacteria Prevotellaceae than WT mice, whereas FMT therapy restored this difference (Fig. 2D). Lachnospiraceae and Ruminococcaceae have been demonstrated to inhibit the production of pro-inflammatory cytokines [38]. At the genus level, WT mice had greater abundances of *Oscillospira*, *Ruminococcus*, [*Ruminococcus*], *Odoribacter*, and *Rikenella* than APP/PS1 mice, whereas APP/PS1 mice had a higher abundance of *Prevotella*. The variance in the APP/PS1+FMT group was similar to that in the WT group, and several organisms, such as *Oscillospira*, were more significantly enriched compared with APP/PS1 (Fig. 2E). To ensure a concise and effective presentation of image information, we conducted a species composition analysis to evaluate differences in species composition among samples. This analysis involved generating heat maps that utilized abundance data for the top 20 genera. As illustrated in Fig. 2F, *Allobaculum*, *Coprococcus*, *Ruminococcus*, and *Clostridium* were enriched in WT mice, and *Desulfovibrio* and *Prevotella* were more abundant in APP/PS1 mice. Furthermore, the abundances of *Roseburia*, *Rikenella*, *Odoribacter*, *Adlercreutzia*, [*Ruminococcus*], *Oscillospira*, *Butyricoccus*, and *Dehalobacterium* were markedly elevated in APP/PS1+FMT mice. Collectively, these findings demonstrated significant modifications in the gut microbiota of APP/PS1 mice, and FMT treatment was found to effectively restore the dysregulated gut microbiota and mitigate the progression of AD.

FMT treatment suppresses inflammation and maintains intestinal barrier integrity by inhibiting TLR4/MyD88/NF- κ B signaling pathway in the colon

Given that FMT could improve cognitive function and memory in APP/PS1 mice, the mechanism of action of FMT was further explored. It has been demonstrated that inflammation is intricately associated with neurodegenerative dementia. An imbalance in the gut microbiota may potentially result in the overexpression of pro-inflammatory factors, thereby triggering neuroinflammation and contributing to the initiation and development of AD [20, 37]. Numerous inflammatory conditions are attributed to NF- κ B, and the activation of MyD88 and NF- κ B by TLR4 can ultimately augment the production of inflammatory cytokines [39]. To verify this theory, the expression

levels of proteins associated with intestinal inflammatory pathways were determined. The expression levels of TLR4 ($P<0.01$), NF- κ B p65 ($P<0.001$), COX2 ($P<0.05$), and MyD88 ($P<0.05$) were higher in APP/PS1 mice than those in WT mice, while the expression levels of TLR4 ($P<0.05$), NF- κ B p65 ($P<0.01$), COX2 ($P<0.05$), and MyD88 ($P<0.05$) were significantly reduced after FMT treatment (Fig. 3A-E). Subsequently, the expression levels of various inflammatory cytokines were examined. The results of Western blot analysis revealed that FMT therapy significantly reduced the expression levels of inflammatory factors IL-6 ($P<0.05$), IL-1 β ($P<0.05$), and TNF- α ($P<0.05$) in APP/PS1 mice (Fig. 3A, F-H). Consistently, the mRNA expression levels of inflammatory factors IL-6 ($P<0.001$), IL-1 β ($P<0.05$), and TNF- α ($P<0.01$) were significantly elevated in APP/PS1 mice compared with those in WT mice, whereas decreased in APP/PS1+FMT mice (Fig. 3I-K). It was postulated that by disrupting the intestinal barrier, pro-inflammatory bacteria could release inflammatory factors into the bloodstream and brain via circulation. The results demonstrated that the expression levels of tight junction (TJ) proteins ZO-1 ($P<0.05$), Occludin ($P<0.001$), and Claudin-1 ($P<0.01$) were significantly downregulated in APP/PS1 mice compared with those in WT mice. However, following FMT treatment, there was a substantial increase in the protein levels of ZO-1 ($P<0.05$) and Claudin-1 ($P<0.05$). Although the expression level of Occludin also increased, the change was not statistically significant (Fig. 4A-D).

Furthermore, hematoxylin and eosin staining of the colon tissue revealed that WT mice had notably higher histological scores compared with APP/PS1 mice. Conversely, APP/PS1 mice exhibited a significantly hyperplastic epithelium and a substantial infiltration of inflammatory cells. In contrast, the intestinal wall of APP/PS1+FMT mice displayed a reduction in thickness, accompanied by a significant alleviation in the infiltration of inflammatory cells (Fig. 4E, F). Following Alcian blue staining, it was indicated that FMT treatment mitigated the disruption of the mucus layer in the colons of APP/PS1 mice (Fig. 4G). The positive area of Alcian blue staining in WT and APP/PS1+FMT mice was significantly larger than that in APP/PS1 mice ($P<0.05$) (Fig. 4H). Taken together, these results demonstrated that FMT treatment suppressed the activation of the TLR4/MyD88/NF- κ B signaling pathway in the colon, preserved the integrity of the intestinal barrier, and ameliorated the progression of intestinal inflammation.

FMT treatment reduces plasma levels of inflammatory factors

To further explore whether inflammatory factors enter the brain through the MGBA to promote the progression of AD, ELISA was employed to detect plasma

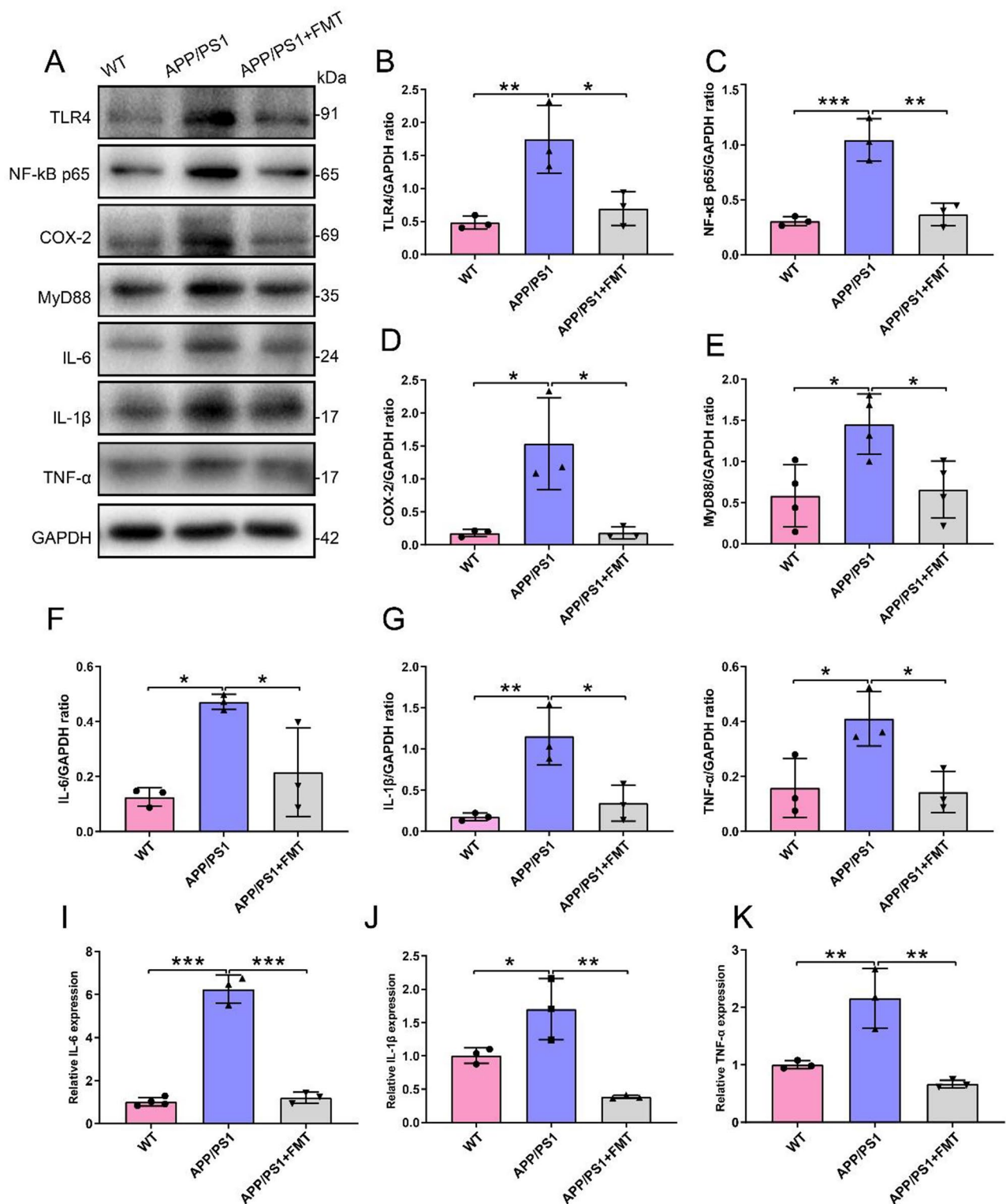


Fig. 3 Effects of FMT treatment on colonic inflammatory signaling pathways in APP/PS1 mice. **(A)** Representative images of TLR4, NF-κB, COX-2, MyD88, IL-6, IL-1β and TNF-α in the colon in Western blot. **(B-H)** Quantitative analysis results of TLR4 ($F = 12.10$; $P = 0.0078$; $df = 8$) ($n = 3$ for each group), NF-κB p65 ($F = 30.76$; $P = 0.0007$; $df = 8$) ($n = 3$ for each group), COX-2 ($F = 11.18$; $P = 0.0095$; $df = 8$) ($n = 3$ for each group), MyD88 ($F = 7.075$; $P = 0.0142$; $df = 11$) ($n = 4$ for each group), IL-6 ($F = 10.41$; $P = 0.0112$; $df = 8$) ($n = 3$ for each group), IL-1β ($F = 14.56$; $P = 0.0050$; $df = 8$) ($n = 3$ for each group) and TNF-α ($F = 7.440$; $P = 0.0237$; $df = 8$) ($n = 3$ for each group) in colon tissue. **(I-K)** Expression of mRNA for IL-6 ($F = 179.8$; $P < 0.0001$; $df = 9$) (WT, $n = 4$; APP/PS1, $n = 3$; APP/PS1 + FMT, $n = 3$), IL-1β ($F = 17.24$; $P = 0.0033$; $df = 8$) ($n = 3$ for each group), and TNF-α ($F = 19.69$; $P = 0.0023$; $df = 8$) ($n = 3$ for each group) in the colon. All data were analyzed by one-way ANOVA, followed by Tukey's multiple comparisons test. Data are expressed as mean \pm SD. * $P < 0.05$; ** $P < 0.01$; *** $P < 0.001$

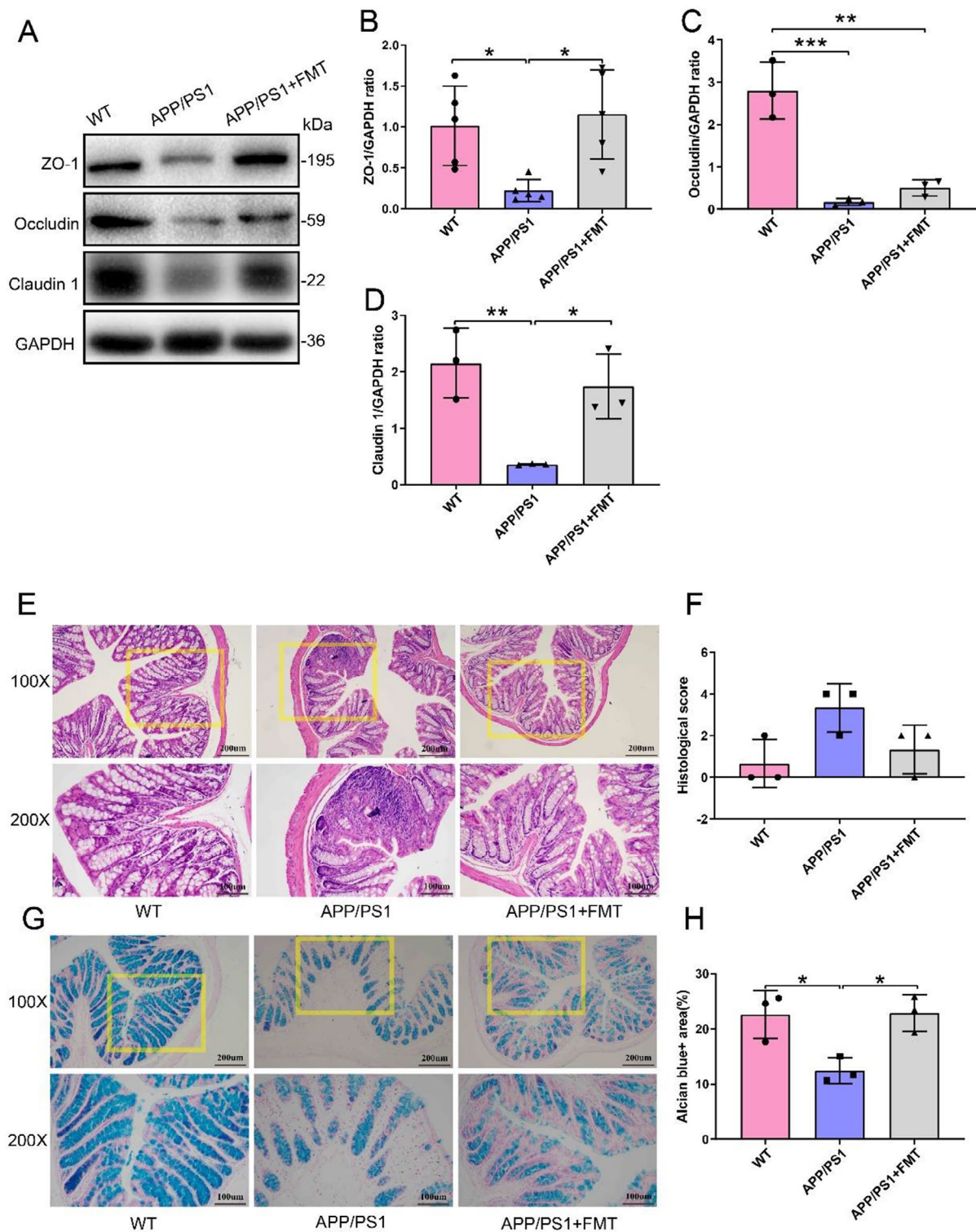


Fig. 4 Effects of FMT treatment on intestinal barrier in APP/PS1 mice. **(A)** Representative images of colonic ZO-1, Occludin and Claudin-1 in the colon from Western blot analysis. **(B-D)** Quantitative analysis of ZO-1 ($F=6.870$; $P=0.0103$; $df=14$) ($n=5$ for each group), Occludin ($F=36.82$; $P=0.0004$; $df=8$) ($n=3$ for each group) and Claudin-1 ($F=11.14$; $P=0.0095$; $df=8$) ($n=3$ for each group) in colon tissue from Western blotting results. **(E, F)** Representative images and histological scores of colonic H&E staining. **(G, H)** Representative images of colonic Alcian blue staining and quantitative analysis of the density with positive areas ($F=9.146$; $P=0.0151$; $df=8$) ($n=3$ for each group). All data were analyzed by one-way ANOVA followed by Tukey's multiple comparisons test. Data are expressed as mean \pm SD. * $P<0.05$; ** $P<0.01$; *** $P<0.001$

cytokine levels. APP/PS1 mice exhibited significantly higher plasma levels of IL-6, IL-1 β , and TNF- α compared with WT mice. However, FMT treatment reduced these levels, indicating a systemic anti-inflammatory effect (Fig. 5A-C).

FMT treatment alleviates brain pathology in APP/PS1 mice and inhibits TLR4/MyD88/NF- κ B signaling pathway thereby suppressing inflammatory factors

Disturbances in the MGBA can promote neuroinflammation, cause nerve damage, and ultimately lead to AD [40]. Neuroinflammation has been proven to play a significant role in the progression of neuropathological alterations in AD [41]. To further investigate whether inflammation could promote pathological changes in AD through activation of the TLR4/MyD88/NF- κ B signaling pathway by the MGBA, the characteristic indicators associated with AD were examined. The results of Western blot assay indicated that APP/PS1 mice had significantly higher levels of amyloid precursor protein (APP) and highly phosphorylated Tau protein (p-Tau) than WT mice and APP/PS1 + FMT mice, however, FMT treatment markedly reversed these changes (Fig. 6A-C). Meanwhile, Congo red staining results of brain sections displayed a large accumulation of β -amyloid plaques in APP/PS1 mice, which were reduced in size and number following FMT treatment, indicating that the pathological features of APP/PS1 mice were improved (Fig. 6D, E). The results of Nissl staining showed that the number of Nissl bodies in the brain of APP/PS1 mice was reduced and loosely arranged, while the number of Nissl bodies was significantly risen and arranged in an orderly manner after FMT treatment, indicating that the function of protein synthesis by neuronal cells became stronger (Fig. 6F, G). In addition, the expression levels of the TLR4/MyD88/NF- κ B signaling pathway-related proteins were further explored. The expression levels of TLR4

($P < 0.05$), NF- κ B p65 ($P < 0.05$), COX-2 ($P < 0.05$), and MyD88 ($P < 0.05$) were significantly higher in the brains of APP/PS1 mice than those in WT mice. FMT treatment remarkably reduced the increased expression levels of pathway-related proteins in APP/PS1 mice (Fig. 7A-E). In addition, the levels of pro-inflammatory cytokines in the brain were examined. Similar to the colon and plasma results, the expression levels of inflammatory factors IL-6 ($P < 0.05$), IL-1 β ($P < 0.05$), and TNF- α ($P < 0.05$) were significantly higher in APP/PS1 mice than those in WT mice, while the expression levels of IL-6 ($P < 0.05$), IL-1 β ($P < 0.01$), and TNF- α ($P < 0.05$) were significantly reduced in APP/PS1 + FMT mice (Fig. 7A, F-H). Similar to the results of Western blotting, the RT-qPCR data demonstrated that FMT treatment reversed the elevation of the levels of pro-inflammatory cytokines (Fig. 7I-K). The above-mentioned findings demonstrated that FMT treatment delayed neuropathological changes in the brains of APP/PS1 mice and inhibited the activation of the TLR4/MyD88/NF- κ B signaling pathway and the production of inflammatory factors, thereby slowing down the progression of AD.

FMT treatment improves short-chain fatty acids levels in the colon and brain of APP/PS1 mice

The expression levels of SCFAs in colonic contents and brain of mice were assessed based on the fact that SCFAs are engaged in MGBA interactions [42]. The heat map showed the greatest variation in butyric, acetic and propionic acids among the fecal samples (Fig. 8A). Compared with the WT group, the expression levels of major SCFAs, such as propionic acid ($P < 0.01$), acetic acid ($P < 0.05$), butyric acid ($P < 0.01$), isobutyric acid ($P < 0.05$), and caproic acid ($P < 0.05$) were significantly reduced in the APP/PS1 group. However, treatment with FMT reversed the reduction in the expression levels of propionic acid ($P < 0.01$), acetic acid ($P < 0.01$), and butyric

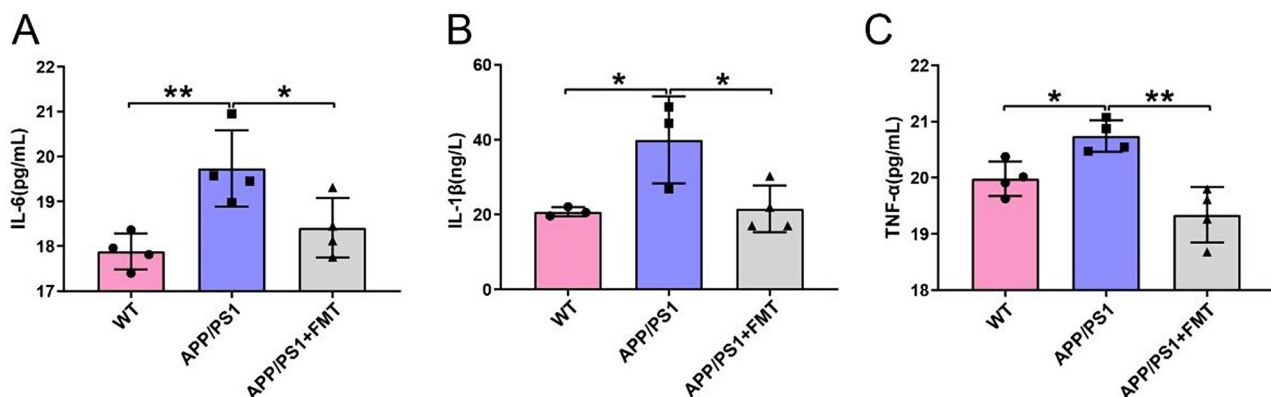


Fig. 5 Alterations of inflammatory cytokine levels in the plasma from APP/PS1 mice after FMT treatment. **(A)** The level of IL-6 ($F = 8.257$; $P = 0.0092$; $df = 11$) ($n = 4$ for each group) in plasma by ELISA kit. **(B)** The level of IL-1 β ($F = 6.622$; $P = 0.0234$; $df = 9$) (WT, $n = 3$; APP/PS1, $n = 3$; APP/PS1 + FMT, $n = 4$) in plasma by ELISA kit. **(C)** The level of TNF- α ($F = 14.20$; $P = 0.0016$; $df = 11$) ($n = 4$ for each group) in plasma by ELISA kit. All data were analyzed by one-way ANOVA, followed by Tukey's multiple comparisons test. Data were expressed as mean \pm SD. * $P < 0.05$; ** $P < 0.01$

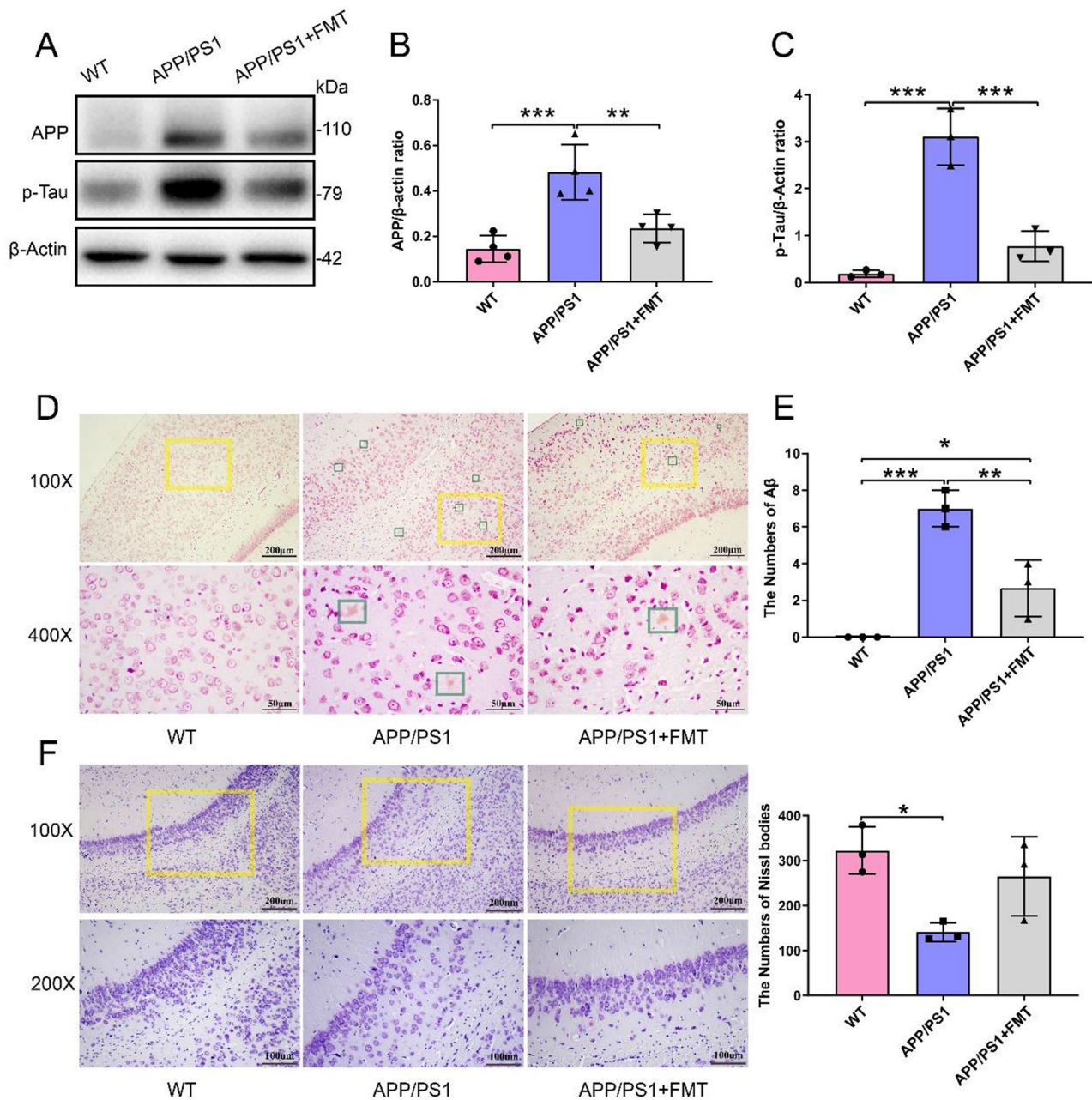


Fig. 6 Influence of FMT treatment on brain pathological changes in APP/PS1 mice. **(A)** Representative images of APP, p-Tau proteins in the hippocampus by Western blot analysis. **(B-C)** Quantification of APP ($F = 16.83$; $P = 0.0009$; $df = 11$) ($n = 4$ for each group), p-Tau ($F = 45.08$; $P = 0.0002$; $df = 8$) ($n = 3$ for each group) proteins in hippocampus according to Western blot results. **(D, E)** Representative images of cortex Congo red staining and the number of A β ($F = 33.70$; $P = 0.0005$; $df = 8$) ($n = 3$ for each group). **(F, G)** Typical images of hippocampal Nissl staining and the number of Nissl bodies ($F = 7.095$; $P = 0.0262$; $df = 8$) ($n = 3$ for each group). All data were analyzed by one-way ANOVA, followed by Tukey's multiple comparisons test. Data were expressed as mean \pm SD. * $P < 0.05$; ** $P < 0.01$; *** $P < 0.001$

acid ($P < 0.01$), and also improved the expression level of valeric acid ($P < 0.05$) (Fig. 8B). However, heat maps of the brain displayed significant differences in the expression levels of SCFAs between the APP/PS1 and WT groups, while the expression levels of propionic acid and butyric acid increased after FMT treatment (Fig. 8C). Propionic acid expression level exhibited the highest variation

among the groups, with the higher expression level in the WT ($P < 0.05$) and APP/PS1+FMT groups ($P < 0.05$) than in the APP/PS1 group, as well as significant differences in acetic acid expression level between the WT and APP/PS1 groups ($P < 0.01$) (Fig. 8D). These results indicated that FMT treatment may affect the disease progression by influencing the expression levels of SCFAs.

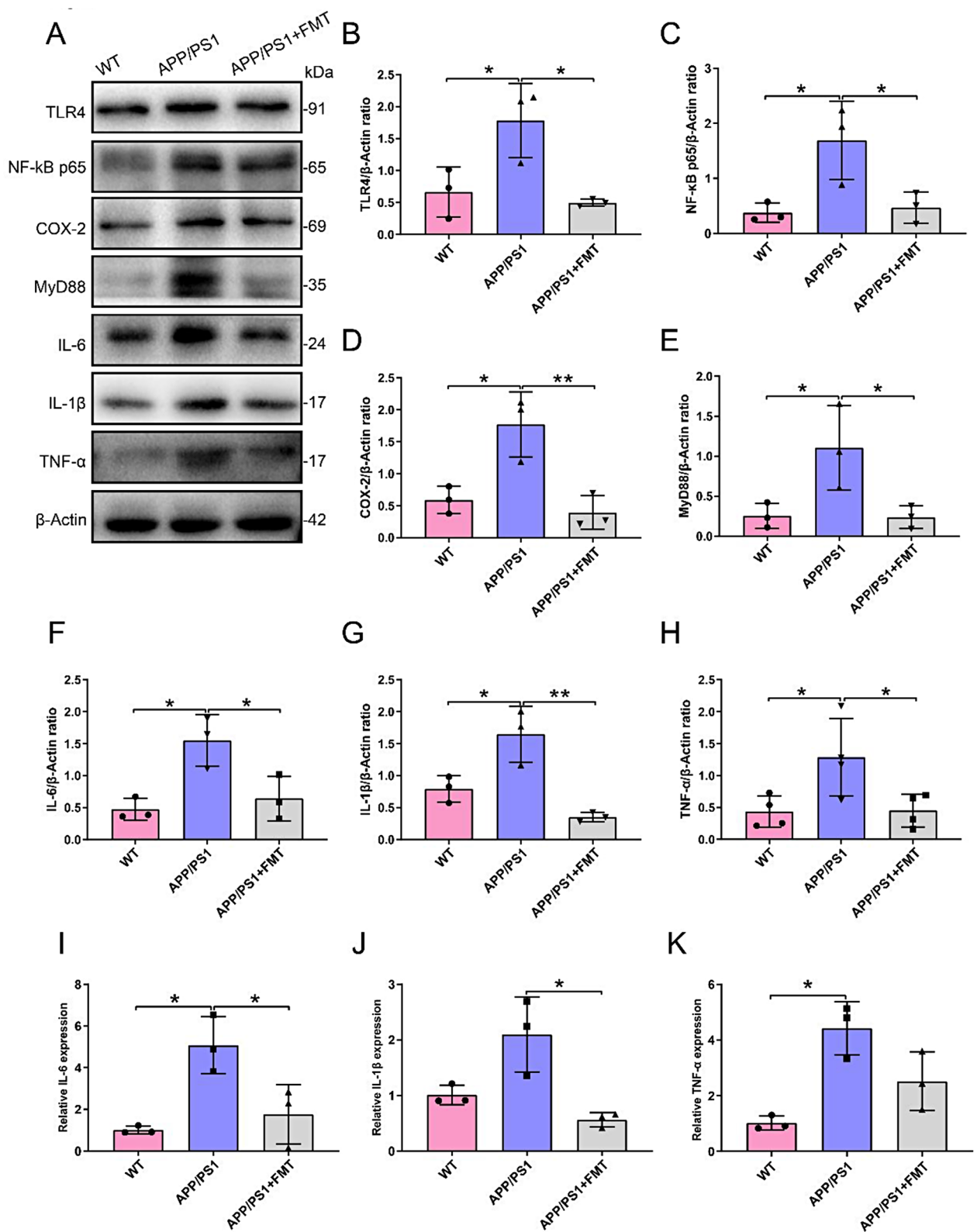


Fig. 7 (See legend on next page.)

(See figure on previous page.)

Fig. 7 Influence of FMT treatment on inflammation-related signaling pathways in the brain of APP/PS1 mice. **(A)** Representative images of hippocampal TLR4, NF- κ B, COX-2, MyD88, IL-6, IL-1 β and TNF- α in Western blot experiments. **(B-H)** Quantification of TLR4 ($F=9.016$; $P=0.0156$; $df=8$) ($n=3$ for each group), NF- κ B p65 ($F=7.862$; $P=0.0211$; $df=8$) ($n=3$ for each group), COX-2 ($F=13.44$; $P=0.0061$; $df=8$) ($n=3$ for each group), MyD88 ($F=6.879$; $P=0.0280$; $df=8$) ($n=3$ for each group), IL-6 ($F=9.593$; $P=0.0135$; $df=8$) ($n=3$ for each group), IL-1 β ($F=16.40$; $P=0.0037$; $df=8$) ($n=3$ for each group) and TNF- α ($F=8.155$; $P=0.0195$; $df=8$) ($n=3$ for each group) proteins in hippocampus according to Western blot results. **(I-K)** Expression of mRNA for IL-6 ($F=10.78$; $P=0.0103$; $df=8$) ($n=3$ for each group), IL-1 β ($F=10.98$; $P=0.0099$; $df=8$) ($n=3$ for each group) and TNF- α ($F=12.53$; $P=0.0072$; $df=8$) ($n=3$ for each group) in the hippocampus. Data were analyzed using one-way ANOVA, followed by Tukey's multiple comparisons test (B-I, K) and Kruskal-Wallis test, followed by Dunn's multiple comparisons test (J). Data were expressed as mean \pm SD. * $P < 0.05$; ** $P < 0.01$

SP inhibits the upregulation of inflammation in FHC cells and BV2 microglia

Notably, SP has anti-inflammatory and neuroprotective effects on the downregulation of the NF- κ B pathway and reducing the production of inflammatory factors [43]. To further investigate the potential mechanisms influencing inflammatory alterations in AD, the viability of FHC and BV2 microglia cells was examined with various concentrations of SP (Fig. 9A, B). The optimal concentration of SP that minimized toxicity was identified to be 5 mM for FHC cells and 500 μ M for BV2 cells. To explore the potential anti-inflammatory effects of SP, FHC cells and BV2 microglial cells were pre-treated with LPS (concentrations of LPS: FHC cells: 20 μ g/ml; microglial cells: 10 μ g/ml), and 5 mM and 500 μ M of SP were subsequently administered. Figure 9C shows the findings of Western blot analysis on FHC cells. It was revealed that the expression levels of TLR4 ($P < 0.05$), NF- κ B p65 ($P < 0.001$), COX2 ($P < 0.05$), and MyD88 ($P < 0.01$) were significantly higher in the LPS-induced group than those in the control group. The expression levels of inflammatory signaling pathway-related proteins and inflammatory factors TLR4 ($P < 0.05$), NF- κ B p65 ($P < 0.01$), COX2 ($P < 0.05$), MyD88 ($P < 0.05$), IL-6 ($P < 0.05$), IL-1 β ($P < 0.01$), and TNF- α ($P < 0.05$) were all downregulated after SP treatment (Fig. 9D-J). The results of BV2 microglia were consistent with those of FHC cells. Western blot analysis indicated significant differences between the control and LPS groups. The expression levels of TLR4 ($P < 0.05$), NF- κ B ($P < 0.05$), COX2 ($P < 0.05$), and MyD88 ($P < 0.05$), along with the pro-inflammatory factors IL-6 ($P < 0.05$), IL-1 β ($P < 0.05$), and TNF- α ($P < 0.05$), exhibited significant reductions after SP treatment (Fig. 9K-R). In conclusion, it was demonstrated that SP could inhibit the TLR4/MyD88/NF- κ B signaling pathway and reduce inflammation production.

Discussion

Through the MGBA, FMT may influence the intestinal microbiota and play an important role in the treatment of neurodegenerative diseases [44]. Kim MS et al. [45] found that fecal microbiota from WT mice might improve pathological characteristics in ADLPAPT mice. FMT treatment, according to Zhao Z et al.'s research [46], may rectify gut microbiota dysbiosis, reduce PD symptoms, and alleviate inflammation. According to the results of

the MWM test, it was indicated that FMT treatment increased the cognitive capacity of APP/PS1 mice, as well as their spatial learning and memory skills (Fig. 1). Furthermore, FMT treatment reduced the expression levels of APP and p-Tau proteins in the brains of APP/PS1 mice (Fig. 6A-C), which are pivotal markers of AD pathology [1]. Histological brain sections corroborated the amelioration of the disease progression in APP/PS1 mice (Fig. 6D-G). These findings suggest that FMT therapy is becoming increasingly important in AD, and it will be a promising treatment option. Despite the fact that FMT treatment can improve the symptoms of AD, its exact mechanism of action has not yet been fully explored [28]. Hence, it is essential to further explore how FMT has therapeutic advantages via acting on the MGBA.

As a result, 16 S rDNA sequencing was conducted on the intestinal contents of mice. It was revealed, in the present study, that *Prevotellaceae* was more prevalent in APP/PS1 mice at the family level, and there was a significant decrease in abundance after FMT treatment (Fig. 2D). *Prevotellaceae* is a classic sign of dysbiosis and has been found to be associated with the production of pro-inflammatory cytokines [47]. Furthermore, after FMT treatment, the abundances of *Lachnospiraceae*, *Ruminococcaceae*, and *Rikenellaceae* increased at the family level in APP/PS1 mice (Fig. 2D). Pro-inflammatory cytokines have a negative relationship with *Lachnospiraceae*, *Ruminococcaceae*, and *Rikenellaceae*, all of which contribute to the production of organismally beneficial SCFAs [38, 48, 49]. In the present study, the abundances of *Prevotella* and *Desulfovibrio* were significantly reduced in APP/PS1 mice at the genus level after FMT treatment, while the abundances of *Oscillospira*, *Odoribacter*, *Rikenella*, and *Roseburia* were elevated (Fig. 2E, F). *Prevotella* has been shown to have inflammatory properties, activating TLR-2 and TLR-4, as well as stimulating epithelial cells to produce inflammatory factors, such as IL-8 and IL-6, indicating that *Prevotella* may be an important pathogen that promotes chronic inflammation [50, 51]. *Desulfovibrio*, which is considered a pro-inflammatory bacterium capable of producing endotoxins, such as LPS, may be positively associated with intestinal inflammation [52]. Hippocampal volume atrophy is linked to dementia. *Odoribacter*, known for its protective effects against cognitive impairment and its association with hippocampal volume, also exhibited anti-inflammatory and

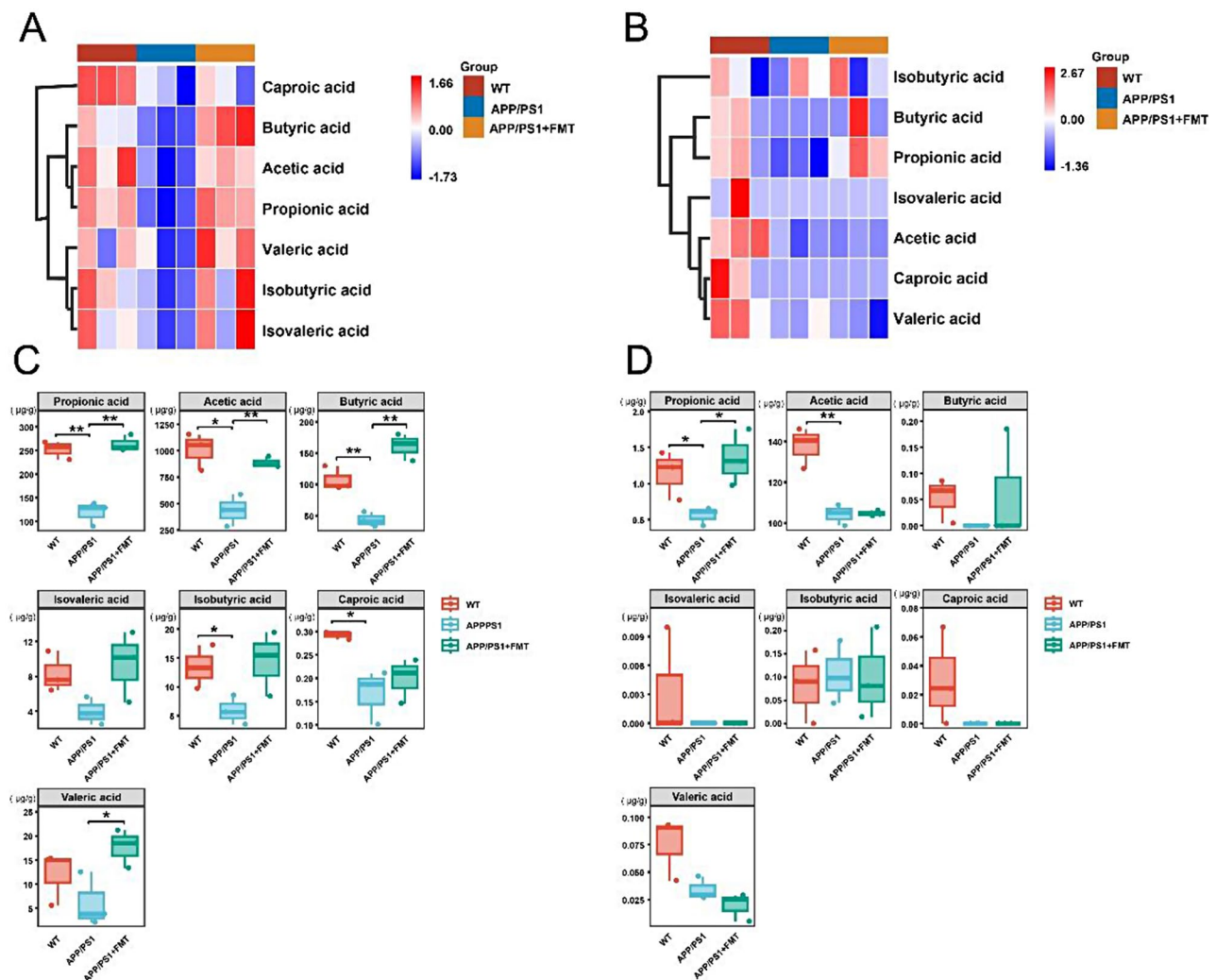


Fig. 8 Impact of FMT treatment on short-chain fatty acid levels in the colon and brain of APP/PS1 mice. **(A)** Heat map of SCFAs in colon contents ($n=4$ for each group). **(B)** Heat map of SCFAs in the brain ($n=3$ for each group). **(C)** Statistical chart of SCFAs in colon contents (Propionic acid: WT vs. APP/PS1, $P=0.0020$, $t=7.204$, $df=4$; APP/PS1 vs. APP/PS1 + FMT, $P=0.0013$, $t=8.039$, $df=4$; Acetic acid: WT vs. APP/PS1, $P=0.0129$, $t=4.271$, $df=4$; APP/PS1 vs. APP/PS1 + FMT, $P=0.0081$, $t=4.897$, $df=4$; Butyric acid: WT vs. APP/PS1, $P=0.0082$, $t=4.873$, $df=4$; APP/PS1 vs. APP/PS1 + FMT, $P=0.0012$, $t=8.267$, $df=4$; Iso-butyric acid: WT vs. APP/PS1, $P=0.0448$, $t=2.884$, $df=4$; Caproic acid: WT vs. APP/PS1, $P=0.0201$, $t=3.743$, $df=4$; Valeric acid: APP/PS1 vs. APP/PS1 + FMT, $P=0.0440$, $t=2.902$, $df=4$) ($n=4$ for each group). **(D)** Statistical chart of SCFAs in the brain (Propionic acid: WT vs. APP/PS1, $P=0.0485$, $t=2.806$, $df=4$; APP/PS1 vs. APP/PS1 + FMT, $P=0.0294$, $t=3.318$, $df=4$; Acetic acid: WT vs. APP/PS1, $P=0.0068$, $t=5.149$, $df=4$) ($n=3$ for each group). Data were analyzed using the two-tailed unpaired t-test **(B, D)**. * $P < 0.05$; ** $P < 0.01$

immunomodulatory properties [53, 54]. Beneficial bacteria, such as *Oscillospira*, *Roseburia*, and *Rikenella* have implications for the amelioration of AD and hold promise as potential therapeutic approaches for the condition [55–57]. It is therefore found that FMT may enhance overall health by regulating bacterial metabolites (e.g., SCFAs) and reducing inflammation.

Chronic inflammation severely damages the nervous system and is a key symptom of neurodegenerative diseases [58], which is associated with cognitive impairment, anxiety, and depression [59]. In the present study, it was revealed that the mRNA and protein expression levels of inflammatory factors in the colon and

hippocampus of APP/PS1 + FMT mice were significantly reduced (Figs. 3 and 7F–K). Meanwhile, FMT treatment resulted in decreased expression levels of pro-inflammatory factors in the plasma (Fig. 5). These findings highlight the pivotal role of inflammation in the pathogenesis of AD and underscore how FMT intervention can counteract the exacerbation of neuroinflammation, ultimately mitigating the progression of inflammation and slowing down the course of the disease.

Intestinal inflammation may play a crucial role in intestinal barrier dysfunction [47]. The integrity of the intestinal barrier is critical for sustaining body health and preventing pathogen invasion. If the intestinal barrier

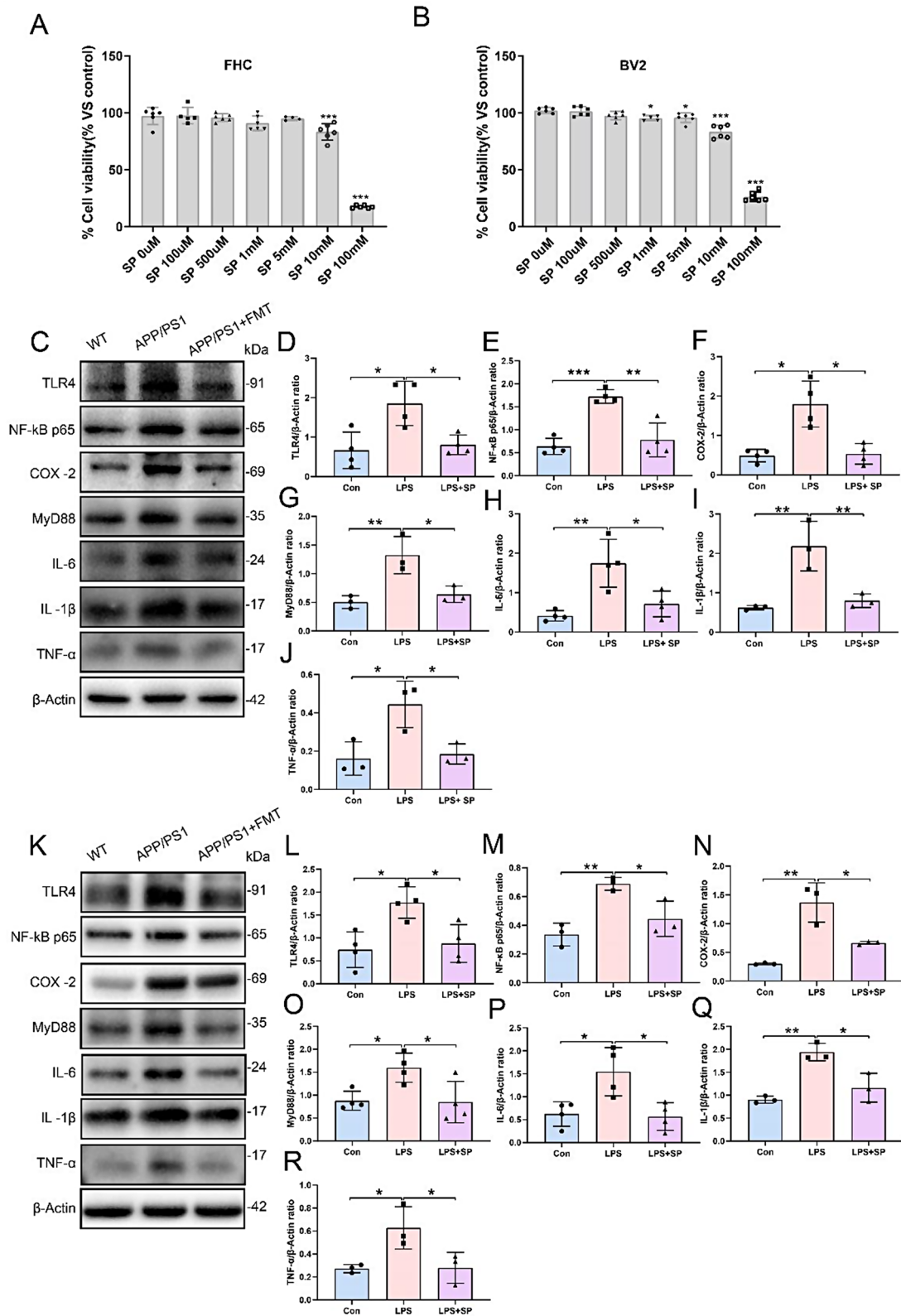


Fig. 9 (See legend on next page.)

(See figure on previous page.)

Fig. 9 Effects of sodium propionate treatment on FHC cells and microglia. **(A)** FHC cell ($n=6$ for each group) viability analysis by CCK8 assay ($F=155.5$; $P<0.0001$; $df=38$). **(B)** BV2 microglia ($n=6$ for each group) viability analysis by CCK8 assay ($F=281.7$; $P<0.0001$; $df=40$). **(C)** Representative images of FHC cell TLR4, NF- κ B p65, COX-2, MyD88, IL-6, IL-1 β and TNF- α in Western blot experiments. **(D-J)** Quantitative analysis results of TLR4 ($F=8.576$; $P=0.0082$; $df=11$) ($n=4$ for each group), NF- κ B ($F=22.28$; $P=0.0003$; $df=11$) ($n=4$ for each group), COX-2 ($F=15.29$; $P=0.0089$) ($n=4$ for each group), MyD88 ($F=12.53$; $P=0.0072$; $df=8$) ($n=3$ for each group), IL-6 ($F=11.75$; $P=0.0031$; $df=11$) ($n=4$ for each group), IL-1 β ($F=15.30$; $P=0.0044$; $df=8$) ($n=3$ for each group) and TNF- α ($F=8.792$; $P=0.0165$; $df=8$) ($n=3$ for each group) on FHC cells. **(K)** Representative images of BV2 microglia TLR4, NF- κ B p65, COX-2, MyD88, IL-6, IL-1 β and TNF- α in Western blot experiments. **(L-R)** Quantitative analysis results of TLR4 ($F=8.567$; $P=0.0083$; $df=11$) ($n=4$ for each group), NF- κ B ($F=12.66$; $P=0.0070$; $df=8$) ($n=3$ for each group), COX-2 ($F=22.59$; $P=0.0016$; $df=8$) ($n=3$ for each group), MyD88 ($F=6.217$; $P=0.0201$; $df=11$) ($n=4$ for each group), IL-6 ($F=8.227$; $P=0.0093$; $df=11$) ($n=4$ for each group), IL-1 β ($F=18.60$; $P=0.0027$; $df=8$) ($n=3$ for each group) and TNF- α ($F=6.929$; $P=0.0276$; $df=8$) ($n=3$ for each group) on BV2 microglia. Data were analyzed using one-way ANOVA, followed by Tukey's multiple comparisons test (**D-E**; **G-J**; **L-R**); one-way ANOVA, followed by Brown-Forsythe and Welch ANOVA test (**F**); one-way ANOVA, followed by Dunnett's multiple comparisons test (**A**, **B**). Data were expressed as mean \pm SD. * $P<0.05$; ** $P<0.01$; *** $P<0.001$

gets damaged, intestinal permeability alters, and viruses and potentially harmful substances enter the bloodstream [60]. This is consistent with plasma ELISA results of the present study, indicating the increased expression levels of inflammatory factors in APP/PS1 mice and a decrease in the expression levels following FMT treatment (Fig. 5). The mucus layer, epithelium, and lamina propria form the majority of the intestinal barrier, and tight junction proteins connect the epithelial cells [60]. Intestinal permeability is determined by the integrity of tight junction proteins, which is required for intestinal barrier function against bacterial and toxic chemical invasion [47]. In the present study, it was revealed that the expression levels of ZO-1, Occludin, and Claudin-1 were remarkably higher in APP/PS1 mice after FMT treatment, demonstrating that intestinal barrier permeability impairment can be improved by restoring the expression levels of tight junction proteins via FMT treatment (Fig. 4A-D). Furthermore, staining of colon sections indicated that FMT treatment reduced inflammatory cell infiltration and mucus layer breakdown (Fig. 4E-H). This is consistent with our previous findings, highlighting the protective effect of FMT on the intestinal barrier by reducing intestinal inflammation, repairing the intestinal barrier, and consequently declining the levels of inflammatory factors in the blood.

To further explore how FMT could mediate the transmission of inflammation to protect the brain through MGBA, the expression levels of SCFAs in colon and hippocampus were detected using GC-MS. SCFAs have long been recognized to reduce the permeability of the intestinal barrier and the BBB, thereby exerting anti-inflammatory effects and reducing LPS invasion into the organism [54, 61]. In the present study, FMT-treated APP/PS1 mice had significantly higher expression levels of major SCFAs, such as propionic acid, butyric acid, and acetic acid in the colon, as well as propionic acid in the hippocampus (Fig. 8). Propionic acid has exhibited anti-inflammatory and anti-cancer properties. Previous studies have demonstrated that propionate could downregulate the TLR4 pathway, inhibit NF- κ B expression level, and consequently decrease the production of

pro-inflammatory cytokines [62]. Phosphorylated NF- κ B has regulatory effects on immunity and inflammation, LPS can trigger NF- κ B p65 transcriptional response and induce pro-inflammatory cytokines secretion through the TLR4-MYD88 pathway [62]. In this study, we selected NF- κ B p65 (RelA) as a marker of pathway activation. Propionate at high doses also reduces LPS-induced inflammatory responses in mice in a TLR-4-dependent manner [63]. Western blot assay was employed to examine the expression levels of proteins associated with the TLR4/MyD88/NF- κ B inflammatory signaling pathway in colon and brain tissues in the present study (Figs. 3 and 7A-E). The results revealed that the TLR4/MyD88/NF- κ B signaling pathway was activated in the colon and brain tissues of APP/PS1 mice, which was suppressed by FMT treatment. Meanwhile, in the relevant cellular experiments, SP processing inhibited the nuclear translocation of the cytosolic factor NF- κ B, inhibited the activation of the TLR4/MyD88/NF- κ B inflammatory signaling pathway, and reduced the production of the pro-inflammatory mediators, such as IL-6, IL-1 β , and TNF- α , as well as COX-2 (Fig. 9). This is consistent with the findings of in vivo mouse experiments, which indicated that the TLR4/MyD88/NF- κ B inflammatory signaling pathway is important in the development of AD. These findings highlight that FMT treatment can enhance the expression levels of SCFAs and reduce the production of inflammatory factors in APP/PS1 mice, restoring the organism's homeostasis and achieving the great therapeutic effect on AD.

The hypothesis posits that gut microbiota dysbiosis may trigger the overgrowth of Gram-negative bacteria, such as *Prevotella* and *Desulfovibrio*, leading to an increased production of LPS. This, in turn, activates the TLR4/MyD88/NF- κ B signaling pathway, facilitating the synthesis of pro-inflammatory molecules, such as IL-6, IL-1 β , and TNF- α . As the intestinal barrier becomes compromised, both LPS and inflammatory agents enter the bloodstream, contributing to systemic inflammation. Subsequently, these inflammatory factors and LPS gain access to the brain through the circulatory system, thereby stimulating the activation of the TLR4/MyD88/NF- κ B signaling pathway and the synthesis of additional

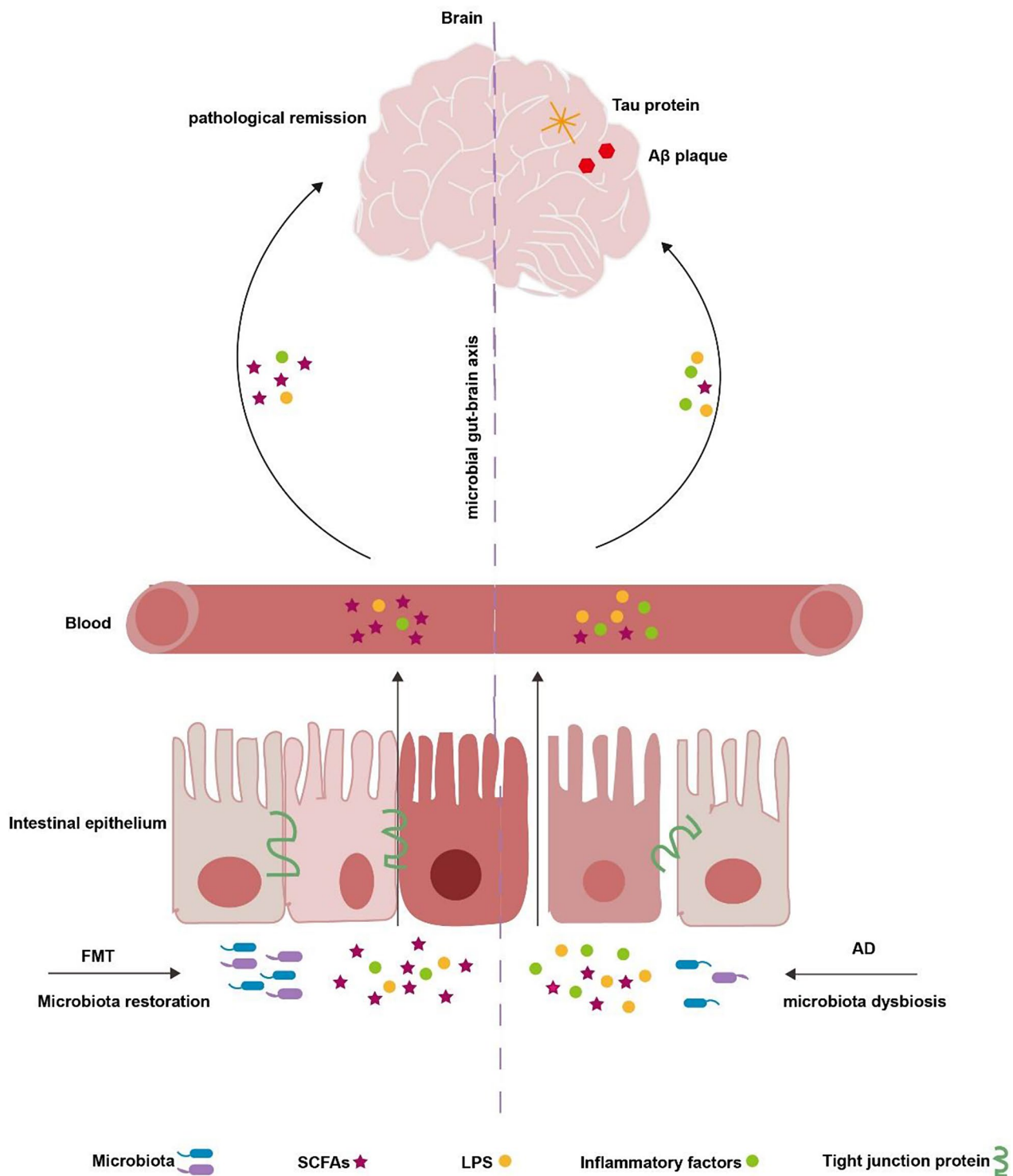


Fig. 10 The pattern of FMT's protective effects on APP/PS1 mice through the microbial-gut-brain axis. In simple terms, FMT treatment works to normalize the imbalances in gut microbiota and short-chain fatty acids (SCFAs), while also slowing down the advancement of pro-inflammatory factors (IL-6, IL-1β, and TNF-α) from the gut to the circulatory system. The reduced levels of these pro-inflammatory factors entering the brain via the gut-brain axis help suppress neuroinflammation, ultimately leading to a delay in the progression of the disease

inflammatory factors, ultimately exacerbating the progression of AD. Conversely, FMT therapy can mitigate

the disease by reducing inflammation levels in APP/PS1 mice via modulation of the MGBA (Fig. 10).

Nonetheless, this study has multiple limitations. In this experiment, we exclusively utilized male mice as the treatment group. However, we acknowledge that we overlooked the variable of sex in our study design. Several studies have highlighted the significance of gender differences, noting that 8-month-old female mice exhibit a higher number of Thioflavin S-positive cortical plaques compared to male mice [64]. Additionally, there are differences in the timeline for plaque accumulation between male and female mice [65]. It is conceivable that hormonal variations and other sex-influenced bodily functions may also play a role in the efficacy of fecal microbiota transplantation (FMT) treatment. The subdiaphragmatic vagus nerve, a key regulatory pathway within the MGBA, has been established as a communication conduit between the gut microbiota and the brain [66]. Wang S et al. [67] demonstrated that *Lactobacillus intestinalis* and *Lactobacillus reuteri* induced depressive behaviors in mice by the vagus nerve, and this effect was not observed in vagotomized mice. Another study found that FMT improved cognitive deficits in T1D mice, and this effect was inhibited by vagotomy or vagal inhibition [68]. Hence, subdiaphragmatic vagus may reduce inflammation in the body by monitoring the gut microbiota and inhibiting the growth of pro-inflammatory bacteria, thereby improving cognitive deficits and delaying aging in mice by enhancing memory through the MGBA. Investigating the impact of the subdiaphragmatic vagus nerve represents a promising direction for the future research in this field.

Conclusions

In conclusion, it was revealed that inflammation plays a critical role in the progression of AD in APP/PS1 mice. FMT treatment delayed the progression of the disease in both intestinal and brain tissues by restoring the intestinal microecology, thereby reducing inflammation mediated by the TLR4/MyD88/NF- κ B signaling pathway.

Supplementary Information

The online version contains supplementary material available at <https://doi.org/10.1186/s12993-024-00265-8>.

Supplementary Material 1

Acknowledgements

Not applicable.

Author contributions

Xiang Li: Funding acquisition, Conceptualization, Supervision, Writing-Reviewing and Editing, Project administration. Qingyong Ding: Data curation, Investigation, Conceptualization, Methodology, Original draft preparation. Xinxin Wan: Investigation, Data curation, Methodology. Qilong Wu: Investigation, Data curation. Shiqing Ye: Data curation, Investigation, Conceptualization. Yongliang Lou: Funding acquisition, Supervision, Project administration.

Funding

This study was supported by the Key Discipline of Zhejiang Province in Medical Technology (First Class, Category A), Industry-university Cooperative education program of Ministry of Education (Grant No. 231104408302408) and Health Project of the Science and Technology Department of Wenzhou (Grant No. Y20220029).

Data availability

The datasets from this study can be accessed in online repositories. Specifically, they are available on the National Center for Biotechnology Information (NCBI) BioProject (<https://www.ncbi.nlm.nih.gov/bioproject>, Accession No. PRJNA1025129), and on the National Center for Biotechnology Information (NCBI) SRA (<https://www.ncbi.nlm.nih.gov/sra>, Accession No. PRJNA1025129). Additionally, the datasets can be found on the National Genomics Data Center (NGDC) China National Center for Bioinformatics (CNGB)/Beijing Institute of Genomics (BIG), Chinese Academy of Sciences (CAS) Open Archive for Miscellaneous Data (OMIX) (<https://ngdc.cncb.ac.cn/omix/>, Accession Nos. PRJCA020313 and PRJCA020312).

Declarations

Ethical approval and consent to participate

All animal protocols were approved by the Experimental Animal Ethics Committee of Wenzhou Medical University (Approval No. wydy2022-0375).

Competing interests

The authors declare no competing interests.

Received: 15 August 2024 / Accepted: 30 December 2024

Published online: 08 January 2025

References

1. Tiwari S, Atluri V, Kaushik A, Yndart A, Nair M. Alzheimer's disease: pathogenesis, diagnostics, and therapeutics. *Int J Nanomed.* 2019;14:5541–54.
2. McKhann GM, Knopman DS, Chertkow H, Hyman BT, Jack CR Jr, Kawas CH, et al. The diagnosis of dementia due to Alzheimer's disease: recommendations from the National Institute on Aging-Alzheimer's Association workgroups on diagnostic guidelines for Alzheimer's disease. *Alzheimers Dement.* 2011;7:263–9.
3. Singh N, Das B, Zhou J, Hu X, Yan R. Targeted BACE-1 inhibition in microglia enhances amyloid clearance and improved cognitive performance. *Sci Adv.* 2022;8:eabo3610.
4. Hampel H, Mesulam MM, Cuello AC, Farlow MR, Giacobini E, Grossberg GT, et al. The cholinergic system in the pathophysiology and treatment of Alzheimer's disease. *Brain.* 2018;141:1917–33.
5. Al-Ghraiyyah NF, Wang J, Alkhalifa AE, Roberts AB, Raj R, Yang E et al. (2022). Glial Cell-Mediated Neuroinflammation in Alzheimer's Disease. *Int J Mol Sci.* 23.
6. Ionescu-Tucker A, Cotman CW. Emerging roles of oxidative stress in brain aging and Alzheimer's disease. *Neurobiol Aging.* 2021;107:86–95.
7. Fang EF, Hou Y, Palikaras K, Adriaanse BA, Kerr JS, Yang B, et al. Mitophagy inhibits amyloid- β and tau pathology and reverses cognitive deficits in models of Alzheimer's disease. *Nat Neurosci.* 2019;22:401–12.
8. Khan S, Barve KH, Kumar MS. Recent advancements in Pathogenesis, Diagnostics and Treatment of Alzheimer's Disease. *Curr Neuropharmacol.* 2020;18:1106–25.
9. Cui W, Sun C, Ma Y, Wang S, Wang X, Zhang Y. Inhibition of TLR4 induces M2 microglial polarization and provides Neuroprotection via the NLRP3 inflammasome in Alzheimer's Disease. *Front Neurosci.* 2020;14:444.
10. Foster JA, Lyte M, Meyer E, Cryan JF. (2016). Gut microbiota and brain function: an Evolving Field in Neuroscience. *Int J Neuropsychopharmacol.* 19.
11. Cryan JF, O'Riordan KJ, Cowan CSM, Sandhu KV, Bastiaanssen TFS, Boehme M, et al. The Microbiota-Gut-Brain Axis. *Physiol Rev.* 2019;99:1877–2013.
12. Sochocka M, Donskow-Lysoniewska K, Diniz BS, Kurpas D, Brzozowska E, Leszek J. The gut microbiome alterations and inflammation-driven pathogenesis of Alzheimer's Disease—a critical review. *Mol Neurobiol.* 2019;56:1841–51.
13. Rutsch A, Kantsjö JB, Ronchi F. The gut-brain Axis: how microbiota and host Inflammation Influence Brain Physiology and Pathology. *Front Immunol.* 2020;11:604179.

14. Jackson HM, Soto I, Graham LC, Carter GW, Howell GR. Clustering of transcriptional profiles identifies changes to insulin signaling as an early event in a mouse model of Alzheimer's disease. *BMC Genomics*. 2013;14:831.
15. Vogt NM, Kerby RL, Dill-McFarland KA, Harding SJ, Merluzzi AP, Johnson SC, et al. Gut microbiome alterations in Alzheimer's disease. *Sci Rep*. 2017;7:13537.
16. Cattaneo A, Cattane N, Galluzzi S, Provasi S, Lopizzo N, Festari C, et al. Association of brain amyloidosis with pro-inflammatory gut bacterial taxa and peripheral inflammation markers in cognitively impaired elderly. *Neurobiol Aging*. 2017;49:60–8.
17. de Theije CG, Wopereis H, Ramadan M, van Eijndthoven T, Lambert J, Knol J, et al. Altered gut microbiota and activity in a murine model of autism spectrum disorders. *Brain Behav Immun*. 2014;37:197–206.
18. Obrenovich MEM. (2018). Leaky Gut, Leaky Brain? *Microorganisms*, 6.
19. Sun MF, Shen YQ. Dysbiosis of gut microbiota and microbial metabolites in Parkinson's Disease. *Ageing Res Rev*. 2018;45:53–61.
20. Bagyinszky E, Giau VV, Shim K, Suk K, An SSA, Kim S. Role of inflammatory molecules in the Alzheimer's disease progression and diagnosis. *J Neurol Sci*. 2017;376:242–54.
21. Wang MM, Miao D, Cao XP, Tan L, Tan L. Innate immune activation in Alzheimer's disease. *Ann Transl Med*. 2018;6:177.
22. Zhao Y, Jaber V, Lukiw WJ. Secretory products of the human GI tract Microbiome and their potential impact on Alzheimer's Disease (AD): detection of Lipopolysaccharide (LPS) in AD Hippocampus. *Front Cell Infect Microbiol*. 2017;7:318.
23. Jin JJ, Kim HD, Maxwell JA, Li L, Fukuchi K. Toll-like receptor 4-dependent upregulation of cytokines in a transgenic mouse model of Alzheimer's disease. *J Neuroinflammation*. 2008;5:23.
24. Smits LP, Bouter KE, de Vos WM, Borody TJ, Nieuwdorp M. Therapeutic potential of fecal microbiota transplantation. *Gastroenterology*. 2013;145:946–53.
25. Vendrik KEW, Ooijevaar RE, de Jong PRC, Laman JD, van Oosten BW, van Hilten JJ, et al. Fecal microbiota transplantation in neurological disorders. *Front Cell Infect Microbiol*. 2020;10:98.
26. Niederwerder MC. Fecal microbiota transplantation as a tool to treat and reduce susceptibility to disease in animals. *Vet Immunol Immunopathol*. 2018;206:65–72.
27. Kim N, Jeon SH, Ju IG, Gee MS, Do J, Oh MS, et al. Transplantation of gut microbiota derived from Alzheimer's disease mouse model impairs memory function and neurogenesis in C57BL/6 mice. *Brain Behav Immun*. 2021;98:357–65.
28. Sun J, Xu J, Ling Y, Wang F, Gong T, Yang C, et al. Fecal microbiota transplantation alleviated Alzheimer's disease-like pathogenesis in APP/PS1 transgenic mice. *Transl Psychiatry*. 2019;9:189.
29. Jing Y, Bai F, Wang L, Yang D, Yan Y, Wang Q, et al. Fecal microbiota transplantation exerts neuroprotective effects in a mouse spinal cord Injury Model by modulating the Microenvironment at the Lesion Site. *Microbiology Spectrum*; 2022. p. 10.
30. Kihara N, de la Fuente SG, Fujino K, Takahashi T, Pappas TN, Mantyh CR. Vanilloid receptor-1 containing primary sensory neurons mediate dextran sulphate sodium induced colitis in rats. *Gut*. 2003;52:713–9.
31. Callahan BJ, McMurdie PJ, Rosen MJ, Han AW, Johnson AJA, Holmes SP. DADA2: high-resolution sample inference from Illumina amplicon data. *Nat Methods*. 2016;13:581–.
32. Han X, Guo J, You Y, Yin M, Ren C, Zhan J, et al. A fast and accurate way to determine short chain fatty acids in mouse feces based on GC-MS. *J Chromatogr B-Analytical Technol Biomed Life Sci*. 2018;1099:73–82.
33. Zhang S, Wang H, Zhu M-J. A sensitive GC/MS detection method for analyzing microbial metabolites short chain fatty acids in fecal and serum samples. *Talanta*. 2019;196:249–54.
34. Hsu Y-L, Chen C-C, Lin Y-T, Wu W-K, Chang L-C, Lai C-H, et al. Evaluation and optimization of Sample handling methods for quantification of short-chain fatty acids in human fecal samples by GC-MS. *J Proteome Res*. 2019;18:1948–57.
35. Bolyen E, Rideout JR, Dillon MR, Bokulich NA, Abnet CC, Al-Ghalith GA et al. (2019). Reproducible, interactive, scalable and extensible microbiome data science using QIIME 2 (vol 37, pg 852, 2019). *Nature Biotechnology*, 37: 1091–1091.
36. Kumar A, Sidhu J, Goyal A, Tsao JW. Alzheimer Disease, StatPearls, StatPearls Publishing Copyright © 2023. StatPearls Publishing LLC., Treasure Island (FL); 2023.
37. Jiang C, Li G, Huang P, Liu Z, Zhao B. The gut microbiota and Alzheimer's Disease. *J Alzheimers Dis*. 2017;58:1–15.
38. Kang C, Wang B, Kaliannan K, Wang X, Lang H, Hui S, et al. Gut microbiota mediates the Protective effects of Dietary Capsaicin against Chronic Low-Grade inflammation and Associated obesity Induced by High-Fat Diet. *mBio*; 2017. p. 8.
39. West AP, Koblansky AA, Ghosh S. Recognition and signaling by toll-like receptors. *Annu Rev Cell Dev Biol*. 2006;22:409–37.
40. Megur A, Baltrikienė D, Bukelskienė V, Burokas A. The Microbiota-Gut-Brain Axis and Alzheimer's Disease. *Neuroinflammation Is to Blame? Nutrients*; 2020. p. 13.
41. Finneran DJ, Nash KR. Neuroinflammation and fractalkine signaling in Alzheimer's disease. *J Neuroinflammation*. 2019;16:30.
42. Silva YP, Bernardi A, Frozza RL. The role of short-chain fatty acids from gut microbiota in Gut-Brain communication. *Front Endocrinol (Lausanne)*. 2020;11:25.
43. Filippone A, Lanza M, Campolo M, Casili G, Paterniti I, Cuzzocrea S et al. (2020). The anti-inflammatory and antioxidant effects of Sodium Propionate. *Int J Mol Sci*, 21.
44. Matheson JT, Holsinger RMD. (2023). The role of fecal microbiota transplantation in the treatment of neurodegenerative diseases: a review. *Int J Mol Sci*, 24.
45. Kim MS, Kim Y, Choi H, Kim W, Park S, Lee D, et al. Transfer of a healthy microbiota reduces amyloid and tau pathology in an Alzheimer's disease animal model. *Gut*. 2020;69:283–94.
46. Zhao Z, Ning J, Bao XQ, Shang M, Ma J, Li G, et al. Fecal microbiota transplantation protects rotenone-induced Parkinson's disease mice via suppressing inflammation mediated by the lipopolysaccharide-TLR4 signaling pathway through the microbiota-gut-brain axis. *Microbiome*. 2021;9:226.
47. Feng J, Li Z, Ma H, Yue Y, Hao K, Li J, et al. Quercetin alleviates intestinal inflammation and improves intestinal functions via modulating gut microbiota composition in LPS-challenged laying hens. *Poult Sci*. 2023;102:102433.
48. Bian X, Wu W, Yang L, Lv L, Wang Q, Li Y, et al. Administration of Akkermansia muciniphila ameliorates Dextran Sulfate Sodium-Induced Ulcerative Colitis in mice. *Front Microbiol*. 2019;10:2259.
49. Liu S, Wu J, Wu Z, Alugongo GM, Zahoor Khan M, Li J, et al. Tributyrin administration improves intestinal development and health in pre-weaned dairy calves fed milk replacer. *Anim Nutr*. 2022;10:399–411.
50. Larsen JM. The immune response to Prevotella bacteria in chronic inflammatory disease. *Immunology*. 2017;151:363–74.
51. Kasselman LJ, Vernice NA, DeLeon J, Reiss AB. The gut microbiome and elevated cardiovascular risk in obesity and autoimmunity. *Atherosclerosis*. 2018;271:203–13.
52. Li Y, Liu M, Liu H, Sui X, Liu Y, Wei X, et al. The anti-inflammatory effect and Mucosal Barrier Protection of Clostridium butyricum RH2 in Ceftriaxone-Induced Intestinal Dysbacteriosis. *Front Cell Infect Microbiol*. 2021;11:647048.
53. Evans TE, Adams HHH, Licher S, Wolters FJ, van der Lugt A, Ikram MK, et al. Subregional volumes of the hippocampus in relation to cognitive function and risk of dementia. *NeuroImage*. 2018;178:129–35.
54. Liang X, Fu Y, Cao WT, Wang Z, Zhang K, Jiang Z, et al. Gut microbiome, cognitive function and brain structure: a multi-omics integration analysis. *Transl Neurodegener*. 2022;11:49.
55. Chen Q, Wu J, Dong X, Yin H, Shi X, Su S, et al. Gut flora-targeted photobio-modulation therapy improves senile dementia in an Aβ-induced Alzheimer's disease animal model. *J Photochem Photobiol B*. 2021;216:112152.
56. Ceccarani C, Bassanini G, Montanari C, Casiraghi MC, Ottaviano E, Morace G et al. (2020). Proteobacteria Overgrowth and Butyrate-Producing Taxa Depletion in the Gut Microbiota of Glycogen Storage Disease Type 1 patients. *Metabolites*, 10.
57. Zhu Y, Liu S, Mei F, Zhao M, Xia G, Shen X. Tilapia nilotica Head lipids improved bone loss by regulating inflammation and serum metabolism through gut microbiota in Ovariectomized rats. *Front Nutr*. 2021;8:792793.
58. DiSabato DJ, Quan N, Godbout JP. Neuroinflammation: the devil is in the details. *J Neurochem*. 2016;139(Suppl 2):136–53.
59. Chesnokova V, Pechnick RN, Wawrowsky K. Chronic peripheral inflammation, hippocampal neurogenesis, and behavior. *Brain Behav Immun*. 2016;58:1–8.
60. König J, Wells J, Cani PD, García-Ródenas CL, MacDonald T, Mercenier A, et al. Human Intestinal Barrier Function in Health and Disease. *Clin Transl Gastroenterol*. 2016;7:e196.
61. Yuan Y, Liu S, Ding X, Li Y, Zhang X, Song H, et al. Early intestinal microbiota changes in aged and adult mice with sepsis. *Front Cell Infect Microbiol*. 2022;12:1061444.
62. Kawasoe J, Uchida Y, Kawamoto H, Miyauchi T, Watanabe T, Saga K, et al. Pro-pionic Acid, Induced in Gut by an Inulin Diet, suppresses inflammation and

- ameliorates Liver Ischemia and Reperfusion Injury in mice. *Front Immunol.* 2022;13:862503.
63. Tian X, Hellman J, Horswill AR, Crosby HA, Francis KP, Prakash A. Elevated gut microbiome-derived propionate levels are Associated with reduced sterile lung inflammation and bacterial immunity in mice. *Front Microbiol.* 2019;10:159.
64. Onos KD, Uyar A, Keezer KJ, et al. Enhancing face validity of mouse models of Alzheimer's disease with natural genetic variation. *PLoS Genet.* 2019;15(5):e1008155. <https://doi.org/10.1371/journal.pgen.1008155>. Published 2019 May 31.
65. Ordóñez-Gutiérrez L, Antón M, Wandosell F. Peripheral amyloid levels present gender differences associated with aging in ABPP/PS1 mice. *J Alzheimers Dis.* 2015;44(4):1063–8. <https://doi.org/10.3233/JAD-141158>.
66. Zhang J, Ma L, Chang L, Pu Y, Qu Y, Hashimoto K. A key role of the subdiaphragmatic vagus nerve in the depression-like phenotype and abnormal composition of gut microbiota in mice after lipopolysaccharide administration. *Transl Psychiatry.* 2020;10:186.
67. Wang S, Ishima T, Zhang J, Qu Y, Chang L, Pu Y, et al. Ingestion of *Lactobacillus intestinalis* and *Lactobacillus reuteri* causes depression- and anhedonia-like phenotypes in antibiotic-treated mice via the vagus nerve. *J Neuroinflammation.* 2020;17:241.
68. Zheng H, Xu P, Jiang Q, Xu Q, Zheng Y, Yan J, et al. Depletion of acetate-producing bacteria from the gut microbiota facilitates cognitive impairment through the gut-brain neural mechanism in diabetic mice. *Microbiome.* 2021;9:145.

Publisher's note

Springer Nature remains neutral with regard to jurisdictional claims in published maps and institutional affiliations.